Spring 2020

# Analysis of energy economy in muon catalyzed fusion considering external x-ray reactivation

Nishant Raghav Pillai



Department:

# ANALYSIS OF ENERGY ECONOMY IN MUON CATALYZED FUSION CONSIDERING EXTERNAL X-RAY REACTIVATION

by

NISHANT RAGHAV PILLAI

A THESIS

Presented to the Faculty of the Graduate School of the

MISSOURI UNIVERSITY OF SCIENCE AND TECHNOLOGY

In Partial Fulfillment of the Requirements for the Degree

MASTER OF SCIENCE IN NUCLEAR ENGINEERING

2020

Approved by:

Joseph Graham, Advisor
Xin Liu
Ayodeji B. Alajo

## ABSTRACT

An analysis of the energy economy of a theoretical muon-catalyzed nuclear fusion system has been made by invoking the use of point kinetic equations, Monte Carlo radiation transport simulations, and from a review of existing literature on muon-catalyzed fusion. An external X-ray reactivation source is proposed as a novel way to increase the number of fusions per muon and thereby overcome the so-called alpha sticking problem that has long been considered the primary impediment to breakeven muon-catalyzed fusion power. Free electron lasers, synchrotrons and Wakefield accelerators are discussed as possible bright X-ray photon sources. The addition of an intense external reactivation source into a deuterium-tritium medium can greatly increase the fusion rate per muon. However, energy breakeven analysis shows that the energy density of a power producing system would need to reach unrealistically high levels in order to maintain the energy cost of the external reactivation source. Thus, external reactivation is not a practical approach to muon-catalyzed fusion.

## ACKNOWLEDGEMENTS

I would like to thank the following individuals for their help and guidance: Dr. Joseph Graham, Kyle Paaren, Alex Swearingen, Ryan Steere, and Seth Kilby.

# TABLE OF CONTENTS

Page

# LIST OF ILLUSTRATIONS

# LIST OF TABLES

# 1. INTRODUCTION

Controlled nuclear fusion has long been a promising but technically challenging endeavor in energy research. Although many efforts to develop controlled fusion power have been made since the first half of the twentieth century, none of them have been able to achieve breakeven, the condition where more energy is generated from fusion than is consumed in reactor systems. That said, technical advances made over the last two decades has renewed interest in the field. Nuclear fusion is the nuclear process in which light nuclei combine to create heavier nuclei, releasing nuclear binding energy in the process. This requires the nuclei to overcome repulsive Coulomb forces, undergo the process of quantum tunneling, and finally fuse together, releasing energy and product nuclei. Quantum tunneling is a phenomenon in which a particle is transmitted through a potential energy barrier, classically, the particle does not have enough kinetic energy to overcome.

In the instance of nuclear fusion, this barrier is the Coulomb barrier, which describes the electrostatic repulsive force between positively charged nuclei. The maximum in the potential energy (i.e. the barrier height) that the classical Coulomb barrier possesses for a two nucleus system is represented by equation (0).

$$E_C = \left(\frac{e^2}{4\pi\varepsilon_0}\right)\frac{Z_1 Z_2}{1.4\left(A_1^{1/3}+A_2^{1/3}\right)} \tag{0}$$

$Z_1$ and $Z_2$ are the atomic numbers of the nuclei, $A_1$ and $A_2$ are the atomic mass numbers. $e$ and $\varepsilon_0$ are the fundamental charge unit and the permittivity of free space, respectively.

For fusion between deuterium and tritium (DT fusion), the resulting minimum kinetic energy required to overcome the Coulomb barrier is 0.44 MeV. If this energy is taken to be the mean kinetic energy of particles in an ideal gas, the temperature of the gas would be 3.43 billion K. This classical analysis, however, does not take into account quantum tunneling, which allows fusion to occur with high probability at lower temperature (on the order of 100 million K). That said, matter at those temperatures is in the plasma state and the technical difficulties of controlled nuclear fusion largely relate to constructing a vessel that can contain, control and heat a plasma.

Typically, plasmas are unavoidable in thermonuclear fusion, the conventional approach to fusion. Thermonuclear plasmas raise the kinetic energy of nuclei to a point where their probability of tunneling in a two-body nuclear collision is high. In a sense, thermonuclear plasmas can be regarded as common as they make up the Sun and other stars. In fact, all elements of the periodic table with masses less than iron are formed in stars through nuclear fusion. Most of the terrestrial approaches to fusion energy generation have relied on recreating a controlled thermonuclear plasma. Due to their high temperature, however, confinement becomes a major technological challenge.

In magnetic confinement fusion, the inherent electromagnetic properties of the plasma state are utilized to confine and manipulate the ionized nuclei in strong magnetic fields. Modern magnetic confinement systems use superconducting electromagnets to produce the strong magnetic fields. Different classes of magnetic confinement devices such as tokamaks, stellarators, and magnetic mirrors differ primarily by the geometric arrangement of the magnetic coils and shape of the resulting magnetic fields. Controlling plasma instabilities has historically been a major challenge in designing these systems.

Instabilities tend to reduce the confinement time, a characteristic time constant that describes the rate of energy leakage from the plasma. Some fusion techniques utilize acute plasma instabilities as driving forces for their fusion reactions such as in field reversed configuration (FRC) devices. Tokamak and stellarators seek to remove them entirely by the manipulation of the magnetic fields used to confine the thermonuclear plasma [1].

The product of the confinement time, plasma temperature and plasma density forms the so-called triple product. For a given plasma temperature, the minimum value of the triple product necessary to generate net energy from fusion and overcome energy losses is referred to as the Lawson criterion. The triple product for several fusion devices is plotted along with the Lawson criterion in Figure 1.1:

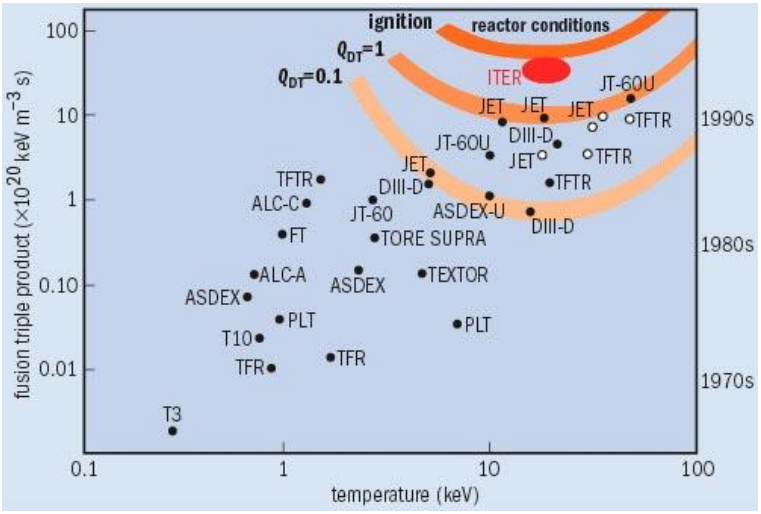


Figure 1.1 Lawson criterion for various fusion devices [2]

Despite the progress that has been made towards surpassing the Lawson criterion, fusion with thermonuclear plasmas is difficult, complex and expensive. Approaches to fusion that eliminate the need for a plasma have the advantage of radically simplifying the confinement systems and removing the problem of plasma instabilities. This in turn minimizes other engineering road blocks holding fusion back such as material damage in the superconducting magnets required to confine the plasma. Maintaining the necessary field strengths for plasma confinement to facilitate fusion is also a problem for an approach involving the use of plasma, as thermal spikes in the superconductor can affect field strength and stability.

Muon-catalyzed fusion is one such approach. As with thermonuclear fusion, the objective in muon-catalyzed fusion is to increase the probability of quantum tunneling in a two-body collision. This is achieved not by increasing the kinetic energies of nuclei entering the collision but by reducing the width of the Coulomb barrier. Solutions to the Schrodinger equation for a barrier potential show that the amplitude of a particle's wavefunction to be on the side of the barrier opposite the incident direction depends on the height and width of the barrier as well as the particle energy.

The greater the height or width, the smaller the amplitude and the lower the probability of tunneling. The height of the barrier is the classical Coulomb barrier energy given in equation (1). The width of the barrier depends on the radial dependence of the charge potential. For an unscreened nucleus, the potential is essentially an infinite range, repulsive Coulomb potential with a central well formed by the strong nuclear force (several fm range). The shape of the wave function in that instance is shown in Figure 1.2:

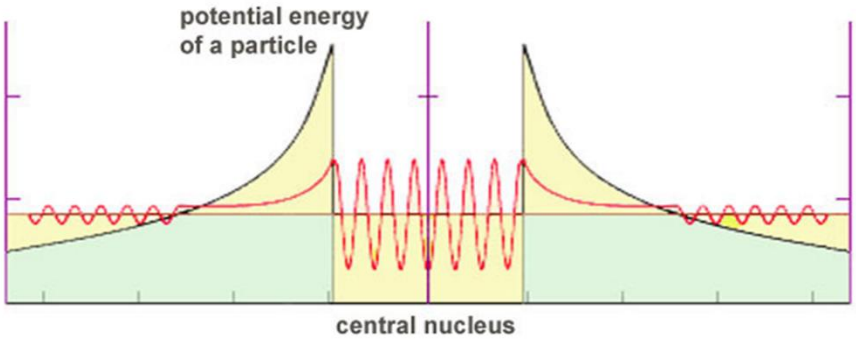


Figure 1.2 Wave function of a charged particle trapped in a nuclear plus Coulomb potential

Muon catalysis utilizes muons to aid in the quantum tunneling that occurs during nuclear fusion by reducing the width of the potential barrier. When muons are bound to nuclei in tight orbitals, they help screen part of the repulsive Coulomb potential at distances much smaller than the atomic radius. This increases the probability that the nuclear wave functions overlap. In fact, electrons also screen the Coulomb potential but only around the Angstrom scale. Muons, being 207 times more massive than electrons form orbitals 207 smaller than electron orbitals. While the screening effect of electrons on nuclear quantum tunneling is negligible at room temperature, muon screening reduces the width of the Coulomb potential enough to dramatically enhance the tunneling rate. Muon catalyzed DT fusion can take place in room temperature and cryogenic temperatures.

A muon is an elementary subatomic particle (μ) similar to the electron. It is classified as a lepton with an electric charge of -1e and a spin of 1/2. Muons are unstable particles that typically decay into an electron or positron and a pair of neutrinos with a 2.2 μs lifetime. As mentioned above, muons can be substituted for electrons in atomic orbitals. The formation of muonic molecules (muomolecules) and ions also occur shortly

after the formation of muonic atoms. The nuclei of these muomolecules are brought closer together but are still separated by a distance of approximately 100 nuclear radii. Because muon orbitals are more tightly bound than electron orbitals, muons easily replace electrons as they can increase total binding energy (Figure 1.3).

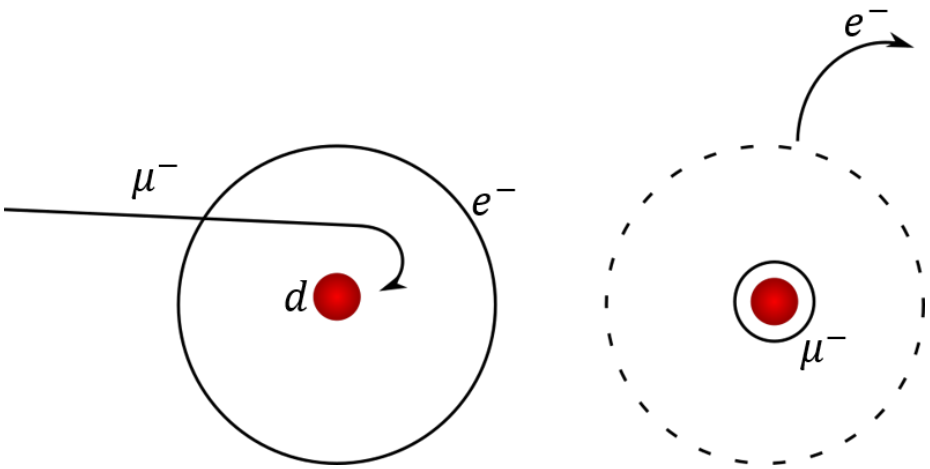


Figure 1.3 Muon capture on a deuterium atom

As with muonic atoms, muomolecules are smaller in size. Muomolecule versions of the diatomic hydrogen molecules ($H_2$, DT, $D_2$) are also approximately 200 times smaller than their electronic counterparts. The reduction of the nuclear separation distance and nuclear charge screening by the muon enhances the tunneling probability and hence catalyzes fusion [3]. The muonic atomic fusion reactions typically present in this process are as follows [4].

$$\mathrm{DT\mu} \rightarrow {}^{4}\mathrm{He} + \mathrm{n} + \mu + 17.58\ \mathrm{MeV} \quad (1)$$

$$\mathrm{DD\mu} \rightarrow {}^{4}\mathrm{He} + \mathrm{n} + \mu + 3.27\ \mathrm{MeV} \quad (2)$$

$$DD\mu \rightarrow T + p + \mu + 4.03\ MeV \quad (3)$$

$$TT\mu \rightarrow {}^{4}He + 2n + \mu + 11.3\ MeV \quad (4)$$

All of these fusion reactions can be expected to occur in DT medium with the DT reactions being the most dominant of the four reactions at low temperatures. The DT reaction creates a neutron, an alpha, and the muon for repeated catalysis. Quantum tunneling occurs on the order of ($10^{-9}$ to $10^{-10}$s) during the fusion process, thus it is possible have the same muon catalyze multiple fusion reactions before it decays [5]. This fusion product (He) however, quenches the catalysis cycle through a process called alpha sticking. Sticking occurs when the muon immediately binds to the alpha particle emerging from the fusion reaction. This effectively prevents the muon from further catalyzing more reactions before it decays away. While the probability of sticking in a particular reaction is small (less than 2%), over several hundred catalysis cycles, a muon is likely to eventually get stuck to an alpha particle and be removed from the system. The complete muon catalysis cycle is represented in Figure 1.4:

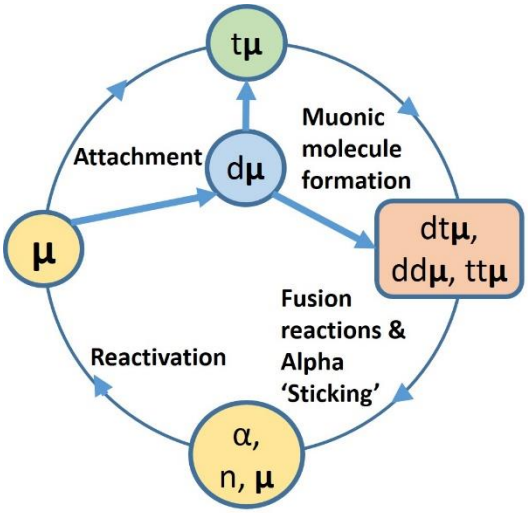


Figure 1.4 Muon catalysis cycle

As mentioned above, muons have a lifetime of 2.2 μs and once stuck to an alpha particle, have a high probability of remaining in orbit until their decay. Thus, alpha sticking is an important loss mechanism of muons from the system. Muonic alpha sticking probabilities have been largely studied theoretically. Within the older Born-Oppenheimer approximation, alpha sticking probabilities of 1.5% have been predicted while in the Green's function Monte Carlo method, the sticking probability is predicted to be around 0.9% [6, 7].

Though an alpha stuck muon has a high probability of remaining trapped to an alpha particle at rest, a moving alpha particle can lose its muon. Reactivation is the phenomenon where an alpha stuck muon gets stripped from a swift muonic alpha particle moving in a medium. There is a 35% chance of the muon reactivating back into the system before the muonic alpha stops and is thermalized. The one must use an effective sticking probability, $\omega_s^{eff}$, to take into account the fraction of reactivated muons, $R$ [8]:

$$(1 - R)\omega_s^o = \omega_s^{eff} \quad (5)$$

$\omega_s^o$ is the sticking probability (without reactivation). Taking into account the 35% probability of reactivation and 1.5% sticking fraction the maximum possible number of fusions per muon has been estimated to be between 150 and 200 fusions per muon before the muon expires or gets stuck. Take the average energy cost to produce a muon as around 5000 MeV [9]. The average energy produced per DT fusion is 17.6 MeV. Thus, each muon must catalyze at least 5000/17.6 = 284 fusion reactions to break even (ignoring losses). Therefore, breakeven appears to be impossible without either reducing the energy cost of the muon or solving the alpha sticking problem.

This work explores the possibility of using an external X-ray source to eject muons stuck in the K-shell of helium. The external reactivation source could be used to repeatedly ionize muons from alpha muonic atoms, thereby reinjecting them into the catalysis cycle. Identifying the conditions under which muon catalyzed fusion with external reactivation can achieve breakeven is the main objective of this research. Figure 1.5 represents muon catalyzed fusion cycle modified with the addition of the novel external reactivation source.

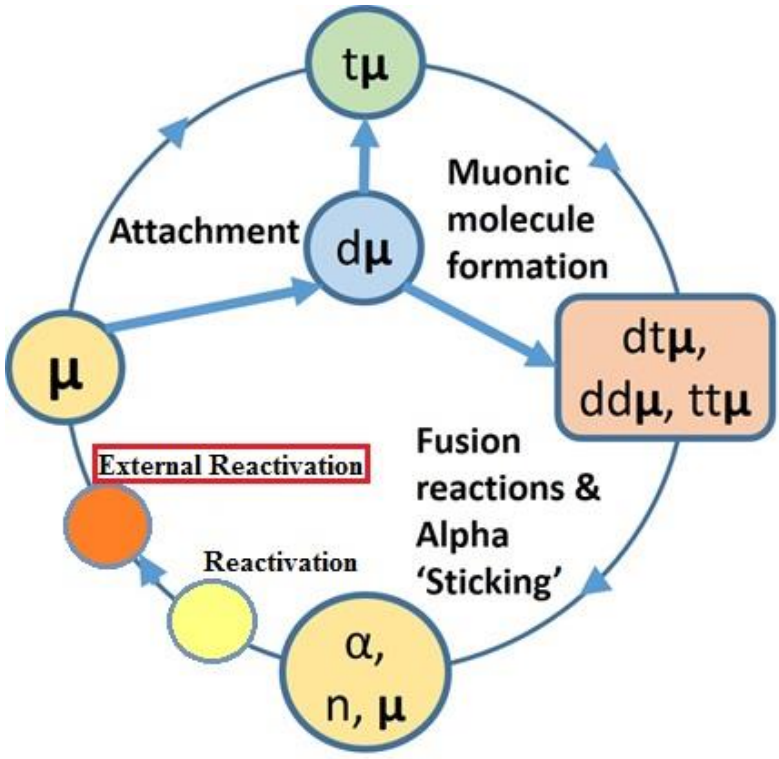


Figure 1.5 Muon catalysis cycle with external reactivation

## 2. MODELING METHODOLOGY

The key distinction between reactivation and external reactivation is that ordinary reactivation is a result of various elastic and inelastic particle collisions in the fuel medium, while external reactivation irradiates the fuel medium with a bright source of photons to ionize alpha stuck muons through the photoelectric (photomuonic) effect and Compton scattering. The insertion of external reactivation is represented in Figure 2.1

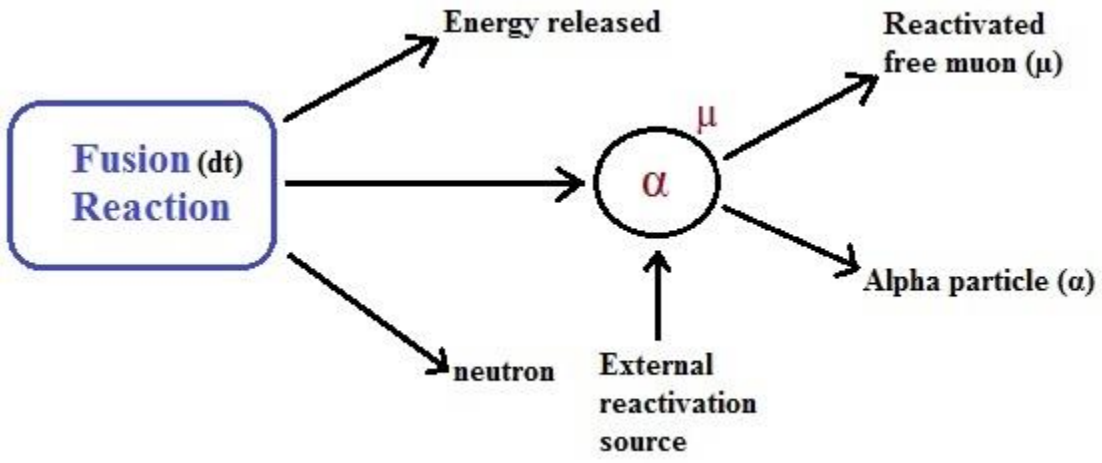


Figure 2.1 External reactivation source on muonic Alpha

In order to determine the feasibility of such a system, predictive and quantitative models are developed to account for the effects of external reactivation. First, point kinetics equations are used to model the populations of free and bound muons in a catalysis cycle in both continuous and pulsed operation. This is covered in Section 3. Second, analytical photomuonic and Compton cross sections are derived in Section 4 and

used to estimate the and necessary flux (fluence) in continuous (pulsed) operation. The selection of an appropriate photon source is also discussed in Section 4. Section 5 presents a criterion for breakeven and discusses the feasibility and realism for a power producing muon catalyzed fusion facility utilizing external reactivation.

# 3. POINT KINETICS MODELLING

A system of point kinetics equations can be established to predict the number of fusions per muon with and without external X-ray reactivation. The population transients from a muon injection pulse will also be used to identify the fluence of X-rays required to achieve breakeven in the muon catalytic cycle. In the equations that follow, variable names and descriptions are given in Table 3.1.

Table 3.1 Definition of variables

| Variable | Definition |
|---|---|
| $N_{d\mu}$ | muonic deuterium number density |
| $\lambda_{d\mu}$ | formation rate of muonic deuterium atom |
| $\lambda_{dd\mu}$ | formation rate of muonic DD molecule |
| $\lambda_{d\mu\rightarrow t\mu}$ | transfer rate of muon from deuterium to tritium |
| $\lambda_{\mu}$ | decay rate of muons |
| $N_{dd\mu}$ | muonic DD molecule number density |
| $\lambda_{dd\mu,f}$ | fusion rate of muonic DD molecule |
| $N_{t\mu}$ | muonic tritium atom number density |
| $\lambda_{t\mu}$ | formation rate of muonic tritium atoms |
| $\lambda_{tt\mu}$ | formation rate of muonic TT molecules |
| $\lambda_{dt\mu}$ | formation rate of muonic DT molecules |
| $N_{tt\mu}$ | muonic TT molecule number density |
| $\lambda_{tt\mu,f}$ | fusion rate of muonic TT molecules |
| $N_{dt\mu}$ | muonic DT molecule number density |
| $N_{\alpha\mu}$ | muonic alpha number density |
| $\omega_{dt}^{eff}$ | effective muon sticking factor of deuteriem tritium atoms |
| $\sigma_{\gamma}$ | photoreactivation cross section of muonic alpha |
| $\phi_{\gamma}$ | flux of photoreactivation source |

The rate of change of the number of free muons in the system, $N_{\mu}$, is.

$$\frac{d}{dt}N_{\mu} = \text{sources} - \text{losses} \tag{6}$$

The sources terms are

$$\text{sources} = S + \left(1 - \omega_{dd}^{eff}\right)\lambda_{dd\mu,f}N_{dd\mu} + \left(1 - \omega_{tt}^{eff}\right)\lambda_{tt\mu,f}N_{tt\mu} + \left(1 - \omega_{dt}^{eff}\right)\lambda_{dt\mu,f}N_{dt\mu} + N_{\alpha\mu}\sigma_{\gamma}\phi_{\gamma} \quad (7)$$

$S$ is the injection rate of muons into the system. The second, third, and fourth terms on the right-hand side of Equation 7 represent the sources of recycled muons from fusion of DT, DD, and TT muomolecules. The terms in parentheses, such as $\left(1 - \omega_{dd}^{eff}\right)$, account for the fraction of muons that leave the reaction without sticking to alpha particles. The last term, the reactivation source term ($N_{\alpha\mu}\sigma_{\gamma}\phi_{\gamma}$), represents the novel external X-ray reactivation source being added to the muon lifecycle. The fusion source terms are based on the number densities of each species multiplied by the fusion rates of each muonic molecule. The loss terms for free muons are

$$\text{losses} = \lambda_{d\mu}N_{\mu} + \lambda_{t\mu}N_{\mu} + \lambda_{\mu}N_{\mu} \quad (8)$$

The losses consist of the number density of the free muons times the formation rates of the muonic atoms. The number densities of the muonic atoms and molecules appearing in equation 6 are coupled to similar equations for each muonic atom/molecule species.

$$\frac{d}{dt}N_{d\mu} = \lambda_{d\mu}N_{\mu} - \lambda_{dd\mu}N_{d\mu} - \lambda_{d\mu\rightarrow t\mu}N_{d\mu} - \lambda_{\mu}N_{d\mu} \quad (9)$$

$$\frac{d}{dt}N_{dd\mu} = \lambda_{dd\mu}N_{d\mu} - \lambda_{dd\mu,f}N_{dd\mu} - \lambda_{\mu}N_{dd\mu} \quad (10)$$

$$\frac{d}{dt}N_{t\mu} = \lambda_{t\mu}N_{\mu} + \lambda_{d\mu\rightarrow t\mu}N_{d\mu} - \lambda_{tt\mu}N_{t\mu} - \lambda_{dt\mu}N_{t\mu} - \lambda_{\mu}N_{t\mu} \quad (11)$$

$$\frac{d}{dt}N_{tt\mu} = \lambda_{tt\mu}N_{t\mu} - \lambda_{tt\mu,f}N_{tt\mu} - \lambda_{\mu}N_{tt\mu} \quad (12)$$

$$\frac{d}{dt}N_{dt\mu} = \lambda_{dt\mu}N_{t\mu} - \lambda_{dt\mu,f}N_{dt\mu} - \lambda_{\mu}N_{dt\mu} \quad (13)$$

$$\frac{d}{dt}N_{\alpha\mu} = \omega_{dt}^{eff}\lambda_{dt\mu,f}N_{dt\mu} - \lambda_{\mu}N_{\alpha\mu} - N_{\alpha\mu}\sigma_{\gamma}\phi_{\gamma} \quad (14)$$

It is assumed that the formation rates of muonic atoms and molecules obey unimolecular kinetics instead of bimolecular kinetics (mass action law). In reality, the formation rates should obey bimolecular kinetics. For example, the formation rate of muonic deuterons is expected to be proportional to the number density of free muons times the number density of electronic deuterium in the fuel mixture. However, as long as the fuel mixture is uniform and the concentrations of muons, muonic atoms and muonic molecules are dilute, the number densities of electronic deuterium and tritium can be treated as approximately constant and therefore incorporated into the rate constants. This approximation makes the system of equations linear and reduces the number of variables.

The first term on the right-hand side of equation 14 describes the fraction of muons that get stuck to alphas that emerge from the fusion reaction and thermalize. The last term describes the external reactivation X-ray source. This later term will be discussed in greater detail in the next section, as it represents the intellectual addition to the cycle that this research will be establishing. Hereafter, ‘external reactivation’ will refer to this third term to avoid confusion with ‘reactivation’ which refers to the natural stripping of muons from energetic muonic helium atoms during the stopping process. Most of the variables appearing in equations 7-14, are values that have been attained from previously established literature on the muon catalytic cycle most of which are from experiments that have been conducted with sources.

The effective sticking rates of muonic molecules were collected from previous modeling studies and implemented in the above kinetics equations. In some cases, these have been experimentally validated. The sticking fractions are represented as percentages, while the formation rates, fusion rates, and decay rate are represented as time constants. These constants are summarized in Table 3.2.

Table 3.2 Values of model parameters

| Constant | Meaning | Typical Values |
|---|---|---|
| $\omega_{dd}^{eff}$ | Effective sticking for DD fusion | 12.2 % [10,11] |
| $\omega_{tt}^{eff}$ | Effective sticking for TT fusion | 14 % [10,11] |
| $\omega_{dt}^{eff}$ | Effective sticking for DT fusion | 0.45 % - 0.65 % [12] |
| $\lambda_{dd\mu,f}$ | DD fusion rate | $10^{10}$ $s^{-1}$ [13] |
| $\lambda_{tt\mu,f}$ | TT fusion rate | $1.5\times10^{7}$ $s^{-1}$ [4] |
| $\lambda_{dt\mu,f}$ | DT fusion rate | $10^{12}$ $s^{-1}$ [5] |
| $\lambda_{d\mu}$ | Muonic D formation | $10^{11}$ $s^{-1}$ [5] |
| $\lambda_{t\mu}$ | Muonic T formation | $10^{11}$ $s^{-1}$ [5] |
| $\lambda_{dd\mu}$ | Muonic DD formation rate | $0.75\times10^{6}$ $s^{-1}$ [4] |
| $\lambda_{tt\mu}$ | Muonic TT formation rate | $1.8\times10^{6}$ $s^{-1}$ [4] |
| $\lambda_{d\mu\rightarrow t\mu}$ | Muon transfer from D to T | $5\times10^{9}$ $s^{-1}$ [5] |
| $\lambda_{dt\mu}$ | Muonic DT formation rate | $7.1\times10^{9}$ $s^{-1}$ [14] |
| $\lambda_{\mu}$ | Muon decay rate | $2.2\times10^{6}$ $s^{-1}$ [14] |

To solve the set of coupled point kinetics equations, they are first Laplace transformed in order to convert the system of differential equations into a system of algebraic equations in frequency space (s). The rate equation for the free muon population becomes

$$sN_{\mu}(s) = \text{sources} - \text{losses} \tag{15}$$

$$\text{sources} = S(s) + \left(1 - \omega_{dd}^{eff}\right)\lambda_{dd\mu,f}N_{dd\mu} + \left(1 - \omega_{tt}^{eff}\right)\lambda_{tt\mu,f}N_{tt\mu} + \left(1 - \omega_{dt}^{eff}\right)\lambda_{dt\mu,f}N_{dt\mu} + N_{\alpha\mu}\sigma_{\gamma}\phi_{\gamma} \quad (16)$$

$$\text{losses} = \lambda_{d\mu}N_{\mu} + \lambda_{t\mu}N_{\mu} + \lambda_{\mu}N_{\mu} \quad (17)$$

Note that each term is implicitly a function of *s* rather than *t*.

The change in number densities of the muonic atoms and molecules is also Laplace transformed into frequency space.

$$sN_{d\mu} = \lambda_{d\mu}N_{\mu} - \lambda_{dd\mu}N_{d\mu} - \lambda_{d\mu\to t\mu}N_{d\mu} - \lambda_{\mu}N_{d\mu} \quad (18)$$

$$sN_{dd\mu} = \lambda_{dd\mu}N_{d\mu} - \lambda_{dd\mu,f}N_{dd\mu} - \lambda_{\mu}N_{dd\mu} \quad (19)$$

$$sN_{t\mu} = \lambda_{t\mu}N_{\mu} + \lambda_{d\mu\to t\mu}N_{d\mu} - \lambda_{tt\mu}N_{t\mu} - \lambda_{dt\mu}N_{t\mu} - \lambda_{\mu}N_{t\mu} \quad (20)$$

$$sN_{tt\mu} = \lambda_{tt\mu}N_{t\mu} - \lambda_{tt\mu,f}N_{tt\mu} - \lambda_{\mu}N_{tt\mu} \quad (21)$$

$$sN_{dt\mu} = \lambda_{dt\mu}N_{t\mu} - \lambda_{dt\mu,f}N_{dt\mu} - \lambda_{\mu}N_{dt\mu} \quad (22)$$

$$sN_{\alpha\mu} = \omega_{dt}^{eff}\lambda_{dt\mu,f}N_{dt\mu} - \lambda_{\mu}N_{\alpha\mu} - N_{\alpha\mu}\sigma_{\gamma}\phi_{\gamma} \quad (23)$$

Next, the number densities for the muonic molecules and muonic atoms are expressed in terms of the number density of free muons by solving the system of equations. This is done to express the kinetic equations in terms of a common variable, $N_{\mu}$. For example, for muonic deuterium-deuterium molecules:

$$N_{d\mu} = \frac{\lambda_{d\mu}N_{\mu}}{s+\lambda_{dd\mu}+\lambda_{d\mu\to t\mu}+\lambda_{\mu}} \quad (24)$$

$$N_{dd\mu} = \frac{\lambda_{dd\mu}N_{d\mu}}{s+\lambda_{dd\mu,f}+\lambda_{\mu}} \quad (25)$$

$$N_{dd\mu} = \left(\frac{\lambda_{dd\mu}}{s+\lambda_{dd\mu,f}+\lambda_{\mu}}\right)\left(\frac{\lambda_{d\mu}}{s+\lambda_{dd\mu}+\lambda_{d\mu\to t\mu}+\lambda_{\mu}}\right)N_{\mu} \quad (26)$$

For muonic tritium-tritium molecules:

$$N_{t\mu} = \frac{\lambda_{t\mu}N_{\mu}}{s+\lambda_{tt\mu}+\lambda_{dt\mu}+\lambda_{\mu}} + \frac{\lambda_{d\mu\to t\mu}N_{d\mu}}{s+\lambda_{tt\mu}+\lambda_{dt\mu}+\lambda_{\mu}} = \left(\frac{1}{s+\lambda_{tt\mu}+\lambda_{dt\mu}+\lambda_{\mu}}\right)\left(\lambda_{t\mu} + \frac{\lambda_{d\mu\to t\mu}\lambda_{d\mu}}{s+\lambda_{dd\mu}+\lambda_{d\mu\to t\mu}+\lambda_{\mu}}\right)N_{\mu} \quad (27)$$

$$N_{tt\mu} = \frac{\lambda_{tt\mu}N_{t\mu}}{s+\lambda_{tt\mu,f}+\lambda_{\mu}} \quad (28)$$

$$N_{tt\mu} = \left(\frac{\lambda_{tt\mu}}{s+\lambda_{tt\mu,f}+\lambda_{\mu}}\right)\left(\frac{1}{s+\lambda_{tt\mu}+\lambda_{dt\mu}+\lambda_{\mu}}\right)\left(\lambda_{t\mu} + \frac{\lambda_{d\mu\to t\mu}\lambda_{d\mu}}{s+\lambda_{dd\mu}+\lambda_{d\mu\to t\mu}+\lambda_{\mu}}\right)N_{\mu} \quad (29)$$

For muonic deuterium-tritium molecules:

$$N_{dt\mu} = \frac{\lambda_{dt\mu}N_{t\mu}}{s+\lambda_{dt\mu,f}+\lambda_{\mu}} \quad (30)$$

$$N_{dt\mu} = \left(\frac{\lambda_{dt\mu}}{s+\lambda_{dt\mu,f}+\lambda_{\mu}}\right)\left(\frac{1}{s+\lambda_{tt\mu}+\lambda_{dt\mu}+\lambda_{\mu}}\right)\left(\lambda_{t\mu} + \frac{\lambda_{d\mu\to t\mu}\lambda_{d\mu}}{s+\lambda_{dd\mu}+\lambda_{d\mu\to t\mu}+\lambda_{\mu}}\right)N_{\mu} \quad (31)$$

For muonic alpha atoms:

$$N_{\alpha\mu} = \frac{\omega_{dt}^{eff}\lambda_{dt\mu,f}N_{dt\mu}}{s+\sigma_{\gamma}\phi_{\gamma}+\lambda_{\mu}} \quad (32)$$

$$N_{\alpha\mu} = \left(\frac{\omega_{dt}^{eff}\lambda_{dt\mu,f}}{s+\sigma_{\gamma}\phi_{\gamma}+\lambda_{\mu}}\right)\left(\frac{\lambda_{dt\mu}}{s+\lambda_{dt\mu,f}+\lambda_{\mu}}\right)\left(\frac{1}{s+\lambda_{tt\mu}+\lambda_{dt\mu}+\lambda_{\mu}}\right)\left(\lambda_{t\mu} + \frac{\lambda_{d\mu\to t\mu}\lambda_{d\mu}}{s+\lambda_{dd\mu}+\lambda_{d\mu\to t\mu}+\lambda_{\mu}}\right)N_{\mu} \quad (33)$$

Next, the sources and losses are written in terms of the formation rates, fusion rates, and free muon number density.

$$\text{sources} = S(s) + \left(1 - \omega_{dd}^{eff}\right)\lambda_{dd\mu,f}\left(\frac{\lambda_{dd\mu}}{s+\lambda_{dd\mu,f}+\lambda_{\mu}}\right)\left(\frac{\lambda_{d\mu}}{s+\lambda_{dd\mu}+\lambda_{d\mu\to t\mu}+\lambda_{\mu}}\right)N_{\mu} + \left(1 - \omega_{tt}^{eff}\right)\lambda_{tt\mu,f}\left(\frac{\lambda_{tt\mu}}{s+\lambda_{tt\mu,f}+\lambda_{\mu}}\right)\left(\frac{1}{s+\lambda_{tt\mu}+\lambda_{dt\mu}+\lambda_{\mu}}\right)\left(\lambda_{t\mu} + \frac{\lambda_{d\mu}}{s+\lambda_{dd\mu}+\lambda_{d\mu\to t\mu}+\lambda_{\mu}}\right)N_{\mu} + \left(1 - \omega_{dt}^{eff}\right)\lambda_{dt\mu,f}\left(\frac{\lambda_{dt\mu}}{s+\lambda_{dt\mu,f}+\lambda_{\mu}}\right)\left(\frac{1}{s+\lambda_{tt\mu}+\lambda_{dt\mu}+\lambda_{\mu}}\right)\left(\lambda_{t\mu} + \frac{\lambda_{d\mu\to t\mu}\lambda_{d\mu}}{s+\lambda_{dd\mu}+\lambda_{d\mu\to t\mu}+\lambda_{\mu}}\right)N_{\mu} + \sigma_{\gamma}\phi_{\gamma}\left(\frac{\omega_{dt}^{eff}\lambda_{dt\mu,f}}{s+\sigma_{\gamma}\phi_{\gamma}+\lambda_{\mu}}\right)\left(\frac{\lambda_{dt\mu}}{s+\lambda_{dt\mu,f}+\lambda_{\mu}}\right)\left(\frac{1}{s+\lambda_{tt\mu}+\lambda_{dt\mu}+\lambda_{\mu}}\right)\left(\lambda_{t\mu} + \frac{\lambda_{d\mu\to t\mu}\lambda_{d\mu}}{s+\lambda_{dd\mu}+\lambda_{d\mu\to t\mu}+\lambda_{\mu}}\right)N_{\mu} \tag{34}$$

$$\text{losses} = \left(\lambda_{d\mu} + \lambda_{t\mu} + \lambda_{\mu}\right)N_{\mu} \tag{35}$$

Pulling out factors of the free muon population gives.

$$\text{sources} = S(s) + \left\{\left(1 - \omega_{dd}^{eff}\right)\lambda_{dd\mu,f}\left(\frac{\lambda_{dd\mu}}{s+\lambda_{dd\mu,f}+\lambda_{\mu}}\right)\left(\frac{\lambda_{d\mu}}{s+\lambda_{dd\mu}+\lambda_{d\mu\to t\mu}+\lambda_{\mu}}\right) + \left(1 - \omega_{tt}^{eff}\right)\lambda_{tt\mu,f}\left(\frac{\lambda_{tt\mu}}{s+\lambda_{tt\mu,f}+\lambda_{\mu}}\right)\left(\frac{1}{s+\lambda_{tt\mu}+\lambda_{dt\mu}+\lambda_{\mu}}\right)\left(\lambda_{t\mu} + \frac{\lambda_{d\mu}}{s+\lambda_{dd\mu}+\lambda_{d\mu\to t\mu}+\lambda_{\mu}}\right) + \left(1 - \omega_{dt}^{eff}\right)\lambda_{dt\mu,f}\left(\frac{\lambda_{dt\mu}}{s+\lambda_{dt\mu,f}+\lambda_{\mu}}\right)\left(\frac{1}{s+\lambda_{tt\mu}+\lambda_{dt\mu}+\lambda_{\mu}}\right)\left(\lambda_{t\mu} + \frac{\lambda_{d\mu\to t\mu}\lambda_{d\mu}}{s+\lambda_{dd\mu}+\lambda_{d\mu\to t\mu}+\lambda_{\mu}}\right) + \sigma_{\gamma}\phi_{\gamma}\left(\frac{\omega_{dt}^{eff}\lambda_{dt\mu,f}}{s+\sigma_{\gamma}\phi_{\gamma}+\lambda_{\mu}}\right)\left(\frac{\lambda_{dt\mu}}{s+\lambda_{dt\mu,f}+\lambda_{\mu}}\right)\left(\frac{1}{s+\lambda_{tt\mu}+\lambda_{dt\mu}+\lambda_{\mu}}\right)\left(\lambda_{t\mu} + \frac{\lambda_{d\mu\to t\mu}\lambda_{d\mu}}{s+\lambda_{dd\mu}+\lambda_{d\mu\to t\mu}+\lambda_{\mu}}\right)\right\}N_{\mu} \tag{36}$$

To simplify the notation, the terms in curly braces are subsumed into a function A(s).

$$\text{sources} = S(s) + A(s)N_{\mu} \tag{37}$$

Similarly, the constant B is used to simply the loss terms.

$$\text{losses} = \text{B}N_{\mu} \tag{38}$$

The free muon population is now given by the single, uncoupled equation:

$$sN_{\mu}(s) = S(s) + \text{A(s)}N_{\mu} - \text{B}N_{\mu} \tag{39}$$

Thus the free muon population in frequency space is:

$$N_\mu(s) = \frac{S(s)}{s+\mathrm{B}-\mathrm{A(s)}} \tag{40}$$

The source term, S(s), in the simplified expression (40) is arbitrary and will be used to represent both a continuous source and a pulsed source. The total fusion rate can be expressed by the following expression:

$$F(s) = \lambda_{dd\mu,f} N_{dd\mu} + \lambda_{tt\mu,f} N_{tt\mu} + \lambda_{dt\mu,f} N_{dt\mu} \tag{41}$$

The total fusion rate in terms of the free muon population can be represented by implementing expressions (26), (29), and (31) into expression (41).

$$F(s) = \left[\lambda_{dd\mu,f}\left(\frac{\lambda_{dd\mu}}{s+\lambda_{dd\mu,f}+\lambda_\mu}\right)\left(\frac{\lambda_{d\mu}}{s+\lambda_{dd\mu}+\lambda_{d\mu\to t\mu}+\lambda_\mu}\right) + \right.$$
$$\lambda_{tt\mu,f}\left(\frac{\lambda_{tt\mu}}{s+\lambda_{tt\mu,f}+\lambda_\mu}\right)\left(\frac{1}{s+\lambda_{tt\mu}+\lambda_{dt\mu}+\lambda_\mu}\right)\left(\lambda_{t\mu} + \frac{\lambda_{d\mu\to t\mu}\lambda_{d\mu}}{s+\lambda_{dd\mu}+\lambda_{d\mu\to t\mu}+\lambda_\mu}\right) +$$
$$\left.\lambda_{dt\mu,f}\left(\frac{\lambda_{dt\mu}}{s+\lambda_{dt\mu,f}+\lambda_\mu}\right)\left(\frac{1}{s+\lambda_{tt\mu}+\lambda_{dt\mu}+\lambda_\mu}\right)\left(\lambda_{t\mu} + \frac{\lambda_{d\mu\to t\mu}\lambda_{d\mu}}{s+\lambda_{dd\mu}+\lambda_{d\mu\to t\mu}+\lambda_\mu}\right)\right] N_\mu \tag{42}$$

By substituting expression (40) into expression (41), the total fusion rate can be written as:

$$F(s) = \left[\lambda_{dd\mu,f}\left(\frac{\lambda_{dd\mu}}{s+\lambda_{dd\mu,f}+\lambda_\mu}\right)\left(\frac{\lambda_{d\mu}}{s+\lambda_{dd\mu}+\lambda_{d\mu\to t\mu}+\lambda_\mu}\right) + \right.$$
$$\lambda_{tt\mu,f}\left(\frac{\lambda_{tt\mu}}{s+\lambda_{tt\mu,f}+\lambda_\mu}\right)\left(\frac{1}{s+\lambda_{tt\mu}+\lambda_{dt\mu}+\lambda_\mu}\right)\left(\lambda_{t\mu} + \frac{\lambda_{d\mu\to t\mu}\lambda_{d\mu}}{s+\lambda_{dd\mu}+\lambda_{d\mu\to t\mu}+\lambda_\mu}\right) +$$
$$\left.\lambda_{dt\mu,f}\left(\frac{\lambda_{dt\mu}}{s+\lambda_{dt\mu,f}+\lambda_\mu}\right)\left(\frac{1}{s+\lambda_{tt\mu}+\lambda_{dt\mu}+\lambda_\mu}\right)\left(\lambda_{t\mu} + \frac{\lambda_{d\mu\to t\mu}\lambda_{d\mu}}{s+\lambda_{dd\mu}+\lambda_{d\mu\to t\mu}+\lambda_\mu}\right)\right] \frac{S(s)}{s+\mathrm{B}-\mathrm{A(s)}} \tag{43}$$

For a continuous muon source starting at time t=0 and injecting muons at a constant rate, S', this becomes:

$$F(s) = \frac{1}{s}\left[\lambda_{dd\mu,f}\left(\frac{\lambda_{dd\mu}}{s+\lambda_{dd\mu,f}+\lambda_{\mu}}\right)\left(\frac{\lambda_{d\mu}}{s+\lambda_{dd\mu}+\lambda_{d\mu\to t\mu}+\lambda_{\mu}}\right)+\right.$$

$$\lambda_{tt\mu,f}\left(\frac{\lambda_{tt\mu}}{s+\lambda_{tt\mu,f}+\lambda_{\mu}}\right)\left(\frac{1}{s+\lambda_{tt\mu}+\lambda_{dt\mu}+\lambda_{\mu}}\right)\left(\lambda_{t\mu}+\frac{\lambda_{d\mu\to t\mu}\lambda_{d\mu}}{s+\lambda_{dd\mu}+\lambda_{d\mu\to t\mu}+\lambda_{\mu}}\right)+$$

$$\left.\lambda_{dt\mu,f}\left(\frac{\lambda_{dt\mu}}{s+\lambda_{dt\mu,f}+\lambda_{\mu}}\right)\left(\frac{1}{s+\lambda_{tt\mu}+\lambda_{dt\mu}+\lambda_{\mu}}\right)\left(\lambda_{t\mu}+\frac{\lambda_{d\mu\to t\mu}\lambda_{d\mu}}{s+\lambda_{dd\mu}+\lambda_{d\mu\to t\mu}+\lambda_{\mu}}\right)\right]\frac{S'}{s+\mathrm{B}-\mathrm{A(s)}} \quad (44)$$

Using the final value theorem, the fusion rate per muon can be attained.

$$\chi = \lim_{s\to 0}\left[\lambda_{dd\mu,f}\left(\frac{\lambda_{dd\mu}}{s+\lambda_{dd\mu,f}+\lambda_{\mu}}\right)\left(\frac{\lambda_{d\mu}}{s+\lambda_{dd\mu}+\lambda_{d\mu\to t\mu}+\lambda_{\mu}}\right)+\right.$$

$$\lambda_{tt\mu,f}\left(\frac{\lambda_{tt\mu}}{s+\lambda_{tt\mu,f}+\lambda_{\mu}}\right)\left(\frac{1}{s+\lambda_{tt\mu}+\lambda_{dt\mu}+\lambda_{\mu}}\right)\left(\lambda_{t\mu}+\frac{\lambda_{d\mu\to t\mu}\lambda_{d\mu}}{s+\lambda_{dd\mu}+\lambda_{d\mu\to t\mu}+\lambda_{\mu}}\right)+$$

$$\left.\lambda_{dt\mu,f}\left(\frac{\lambda_{dt\mu}}{s+\lambda_{dt\mu,f}+\lambda_{\mu}}\right)\left(\frac{1}{s+\lambda_{tt\mu}+\lambda_{dt\mu}+\lambda_{\mu}}\right)\left(\lambda_{t\mu}+\frac{\lambda_{d\mu\to t\mu}\lambda_{d\mu}}{s+\lambda_{dd\mu}+\lambda_{d\mu\to t\mu}+\lambda_{\mu}}\right)\right]\frac{1}{s+\mathrm{B}-\mathrm{A(s)}} \quad (45)$$

For a pulsed system where $S_0$ muons are injected in a delta function pulse at time t=0, the expression becomes:

$$F(s) = \left[\lambda_{dd\mu,f}\left(\frac{\lambda_{dd\mu}}{s+\lambda_{dd\mu,f}+\lambda_{\mu}}\right)\left(\frac{\lambda_{d\mu}}{s+\lambda_{dd\mu}+\lambda_{d\mu\to t\mu}+\lambda_{\mu}}\right)+\right.$$

$$\lambda_{tt\mu,f}\left(\frac{\lambda_{tt\mu}}{s+\lambda_{tt\mu,f}+\lambda_{\mu}}\right)\left(\frac{1}{s+\lambda_{tt\mu}+\lambda_{dt\mu}+\lambda_{\mu}}\right)\left(\lambda_{t\mu}+\frac{\lambda_{d\mu\to t\mu}\lambda_{d\mu}}{s+\lambda_{dd\mu}+\lambda_{d\mu\to t\mu}+\lambda_{\mu}}\right)+$$

$$\left.\lambda_{dt\mu,f}\left(\frac{\lambda_{dt\mu}}{s+\lambda_{dt\mu,f}+\lambda_{\mu}}\right)\left(\frac{1}{s+\lambda_{tt\mu}+\lambda_{dt\mu}+\lambda_{\mu}}\right)\left(\lambda_{t\mu}+\frac{\lambda_{d\mu\to t\mu}\lambda_{d\mu}}{s+\lambda_{dd\mu}+\lambda_{d\mu\to t\mu}+\lambda_{\mu}}\right)\right]\frac{S_0}{s+\mathrm{B}-\mathrm{A(s)}} \quad (46)$$

Rather than use the final value theorem, which will merely confirm that the fusion rate falls to zero long after the pulse, the function should be integrated over time, to determine, $G(t)$, the cumulative number of fusions following a pulse.

$$G(t) = \int_0^t F(t')dt \quad (47)$$

In frequency space, the cumulative number of fusions is:

$$G(s) = \frac{1}{s}\left[\lambda_{dd\mu,f}\left(\frac{\lambda_{dd\mu}}{s+\lambda_{dd\mu,f}+\lambda_{\mu}}\right)\left(\frac{\lambda_{d\mu}}{s+\lambda_{dd\mu}+\lambda_{d\mu\to t\mu}+\lambda_{\mu}}\right)+\right.$$

$$\lambda_{tt\mu,f}\left(\frac{\lambda_{tt\mu}}{s+\lambda_{tt\mu,f}+\lambda_{\mu}}\right)\left(\frac{1}{s+\lambda_{tt\mu}+\lambda_{dt\mu}+\lambda_{\mu}}\right)\left(\lambda_{t\mu}+\frac{\lambda_{d\mu\to t\mu}\lambda_{d\mu}}{s+\lambda_{dd\mu}+\lambda_{d\mu\to t\mu}+\lambda_{\mu}}\right)+$$

$$\left.\lambda_{dt\mu,f}\left(\frac{\lambda_{dt\mu}}{s+\lambda_{dt\mu,f}+\lambda_{\mu}}\right)\left(\frac{1}{s+\lambda_{tt\mu}+\lambda_{dt\mu}+\lambda_{\mu}}\right)\left(\lambda_{t\mu}+\frac{\lambda_{d\mu\to t\mu}\lambda_{d\mu}}{s+\lambda_{dd\mu}+\lambda_{d\mu\to t\mu}+\lambda_{\mu}}\right)\right]\frac{S_0}{s+\mathrm{B}-\mathrm{A(s)}} \quad (48)$$

For large t, $G(t)$ approaches the total number of fusions per pulse. Dividing both sides by $S_0$ and using the final value theorem gives:

$$\chi = \lim_{s\to 0}\left[\lambda_{dd\mu,f}\left(\frac{\lambda_{dd\mu}}{s+\lambda_{dd\mu,f}+\lambda_{\mu}}\right)\left(\frac{\lambda_{d\mu}}{s+\lambda_{dd\mu}+\lambda_{d\mu\to t\mu}+\lambda_{\mu}}\right)+\right.$$

$$\lambda_{tt\mu,f}\left(\frac{\lambda_{tt\mu}}{s+\lambda_{tt\mu,f}+\lambda_{\mu}}\right)\left(\frac{1}{s+\lambda_{tt\mu}+\lambda_{dt\mu}+\lambda_{\mu}}\right)\left(\lambda_{t\mu}+\frac{\lambda_{d\mu\to t\mu}\lambda_{d\mu}}{s+\lambda_{dd\mu}+\lambda_{d\mu\to t\mu}+\lambda_{\mu}}\right)+$$

$$\left.\lambda_{dt\mu,f}\left(\frac{\lambda_{dt\mu}}{s+\lambda_{dt\mu,f}+\lambda_{\mu}}\right)\left(\frac{1}{s+\lambda_{tt\mu}+\lambda_{dt\mu}+\lambda_{\mu}}\right)\left(\lambda_{t\mu}+\frac{\lambda_{d\mu\to t\mu}\lambda_{d\mu}}{s+\lambda_{dd\mu}+\lambda_{d\mu\to t\mu}+\lambda_{\mu}}\right)\right]\frac{1}{s+\mathrm{B}-\mathrm{A(s)}} \quad (49)$$

This is precisely the same result as for a continuous source. This is a consequence of the linearity of the kinetics equations.

The external reactivation X-ray source in expression (14) was assumed continuous. To investigate the kinetics of a system with both pulsed muons and pulsed X-rays, it helps to study the solution for the number density of the muonic alpha in the time domain with the continuous external reactivation source turned off. The expression for the muonic alpha is:

$$N_{\alpha\mu} = \left(\frac{\omega_{dt}^{eff}\lambda_{dt\mu,f}}{s+\lambda_{\mu}}\right)\left(\frac{\lambda_{dt\mu}}{s+\lambda_{dt\mu,f}+\lambda_{\mu}}\right)\left(\frac{\lambda_{t\mu}}{s+\lambda_{tt\mu}+\lambda_{dt\mu}+\lambda_{\mu}}\right)\frac{S(s)}{s+B-A(s)} \quad (50)$$

Equation (50) can be simplified using partial fraction expansion and then inverse Laplace transformed yielding the kinetics of the alpha stuck muons following a muon

pulse. The partial fraction expansion was performed using the Maxima software. The results, though too lengthy to represent here, were converted into a Matlab script that performs the inverse Laplace transform and plots the time domain transients.

The total fusions per muon following a muon pulse is shown in Figure 3.1. The maximum fusions per muon is between 150-200 which agrees with previous computational and experimental literature. Based on the energy cost per muon at current muon sources, each muon would need to catalyze more than 300 fusion events ($\chi > 300$) in order to break even [15]. Thus without external reactivation, the point kinetics model confirms that muon catalyzed fusion is unlikely to reach breakeven conditions.

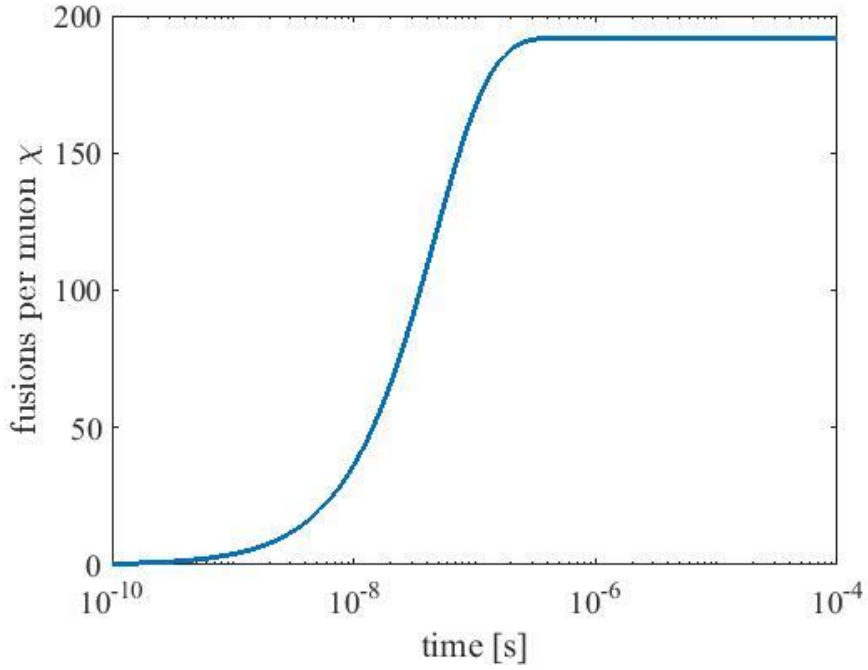


Figure 3.1 Fusions per muon following muon pulse

On the other hand, alpha stuck muons are present in high concentrations at some moment following the muon injection pulse. Figure 3.2 shows the muonic alpha population transient following a muon pulse at time t=0. At about 0.2 μs after injection, roughly 90% of the muons in the system are stuck to alpha particles. This suggests that a brilliant photon pulse, delayed from the initial muon pulse by 0.2 μs has the potential to reactivate a large fraction of the initial muons.

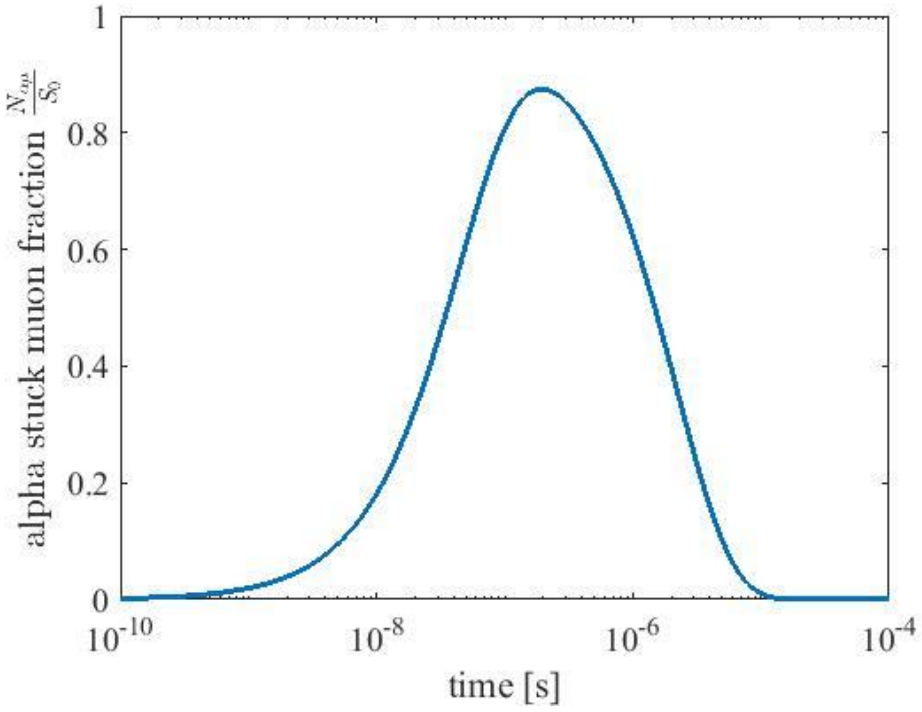


Figure 3.2 Fraction of muons stuck to alphas following a muon pulse

# 4. REACTIVATION ANALYSIS

In order to identify the design requirements of the external reactivation photon source, three parameters need to be identified:

i. The cross section for muonic alpha photoionization.

ii. The photon flux or fluence required to achieve a specified muon reactivation rate.

iii. The reaction rate required to eject enough muons to significantly increase the number of fusions per muon.

The ionization cross section of the muonic alpha consists of photoelectric (photomuonic) absorption and a Compton scattering components. In order to calculate the photoreactivation rate, the differential photoelectric cross sections and differential incoherent (Compton) scattering cross sections need to be determined.

## 4.1. PHOTOELECTRIC ABSORPTION

The differential cross section for photoelectric absorption is based off of harmonic perturbation theory. It is derived in a similar manner to [16] except for muons instead of electrons. From first order time-dependent perturbation theory, the differential cross section, $d\sigma_{i\to f}$ can be attained for an atom with initial state $i$ and energy $E_i$ absorbing a photon of energy $\hbar\omega$ and leaving the atom in final state $f$ with energy $E_f$ by the following relation:

$$d\sigma_{i\to f} = \frac{4\pi^2\alpha\hbar}{\mu^2\omega}\left|\left\langle f\left|e^{i\left(\frac{\omega}{c}\right)(\hat{\mathbf{n}}\cdot\mathbf{x})}\hat{\boldsymbol{\varepsilon}}\cdot\mathbf{p}\right|i\right\rangle\right|^2\delta\left(E_f - E_i - \hbar\omega\right) \tag{51}$$

$\alpha$ is the fine structure constant (~1/137), $\hbar$ is the reduced Planck's constant, $\omega$ is the frequency of the incident photon and $c$ is the speed of light. It can be assumed that the photon is plane polarized with photon wave vector $\mathbf{k}_\gamma = \frac{\omega}{c}\hat{\mathbf{n}}$ and polarization vector $\hat{\boldsymbol{\varepsilon}}\cdot\mathbf{p}$ is the electron (muon) momentum operator. $\mu$ is the reduced mass of the atom, i.e.

$$\frac{1}{\mu} = \frac{1}{M} + \frac{1}{m} \tag{52}$$

where $M$ is the mass of the nucleus and $m$ is the mass of the electron (muon). For K-shell photoelectric absorption it is suitable to define the initial state as consisting of a ground state atom and a plane wave photon, $|0, \mathbf{k}_\gamma\rangle$ (0 denotes the atom ground state). The final state has an outgoing electron (muon) plane wave with wave vector $\mathbf{k}_e$. With those substitutions the differential cross section becomes:

$$d\sigma_{pe} = \frac{4\pi^2\alpha}{\mu^2\omega v_e}\left|\left\langle \mathbf{k}_e\left| e^{i\left(\frac{\omega}{c}\right)(\hat{\mathbf{n}}\cdot\mathbf{x})}\hat{\boldsymbol{\varepsilon}}\cdot\mathbf{p}\right|0,\mathbf{k}_\gamma\right\rangle\right|^2 \delta\left(k_e - \frac{1}{\hbar}\sqrt{2\mu(E_0+\hbar\omega)}\right) \tag{53}$$

Using the box-normalization procedure and writing the differential cross section as a function of solid angle for the outgoing electron (muon) [17]. Thus:

$$\frac{d\sigma_{pe}}{d\Omega} = \frac{4\pi^2\alpha k_e^2}{\mu^2\omega v_e}\left|\left\langle \mathbf{k}_e\left| e^{i\left(\frac{\omega}{c}\right)(\hat{\mathbf{n}}\cdot\mathbf{x})}\hat{\boldsymbol{\varepsilon}}\cdot\mathbf{p}\right|0,\mathbf{k}_\gamma\right\rangle\right|^2 \left(\frac{L}{2\pi}\right)^3; \quad k_e = \frac{1}{\hbar}\sqrt{2\mu(E_0+\hbar\omega)} \tag{54}$$

Where $L$ is the length of the box. In terms of the ground state wave function $\psi_0(x)$ the inner bracket can be written as

$$\left\langle \mathbf{k}_e\left| e^{i\left(\frac{\omega}{c}\right)(\hat{\mathbf{n}}\cdot\mathbf{x})}\hat{\boldsymbol{\varepsilon}}\cdot\mathbf{p}\right|0,\mathbf{k}_\gamma\right\rangle = \frac{\hbar\hat{\boldsymbol{\varepsilon}}\cdot\mathbf{k}_e}{L^{\frac{3}{2}}}\int d^3x\, e^{-i\mathbf{q}\cdot\mathbf{x}}\psi_0(x) \tag{55}$$

$\mathbf{q}$ is the scattering vector

$$\mathbf{q} = \mathbf{k}_e - \mathbf{k}_\gamma = \mathbf{k}_e - \left(\frac{\omega}{c}\right)\hat{\mathbf{n}} \tag{56}$$

A simple and convenient choice of the ground state wave function is the ground state wave function of the hydrogen-like atom with nuclear charge $Z$

$$\psi_0(x) = \frac{1}{\sqrt{4\pi}}\left(\frac{2Z}{a_\mu}\right)^{\frac{3}{2}} \exp\left(-\frac{Zr}{a_\mu}\right) \tag{57}$$

with eigenenergy $E_0 = -\frac{\mu c^2 Z^2 \alpha^2}{2}$. $a_\mu$ is the Bohr radius adjusted for the reduced mass of the atom

$$a_\mu = \frac{\hbar c}{\mu c^2 \alpha} = \frac{m_e}{\mu} a_0 \tag{58}$$

Performing the integral gives

$$\int d^3x\, e^{-i\mathbf{q}\cdot\mathbf{x}}\psi_0(x) = \sqrt{64\pi}\left(\frac{Z}{a_\mu}\right)^{\frac{5}{2}} \frac{1}{\left[\left(\frac{Z^2}{a_\mu^2}\right)+q^2\right]^2} \tag{59}$$

Thus

$$\left\langle \mathbf{k}_e \middle| e^{i\left(\frac{\omega}{c}\right)(\hat{\mathbf{n}}\cdot\mathbf{x})}\hat{\boldsymbol{\varepsilon}}\cdot\mathbf{p} \middle| 0, \mathbf{k}_\gamma \right\rangle = \frac{\hbar\hat{\boldsymbol{\varepsilon}}\cdot\mathbf{k}_e}{L^{\frac{3}{2}}}\sqrt{64\pi}\left(\frac{Z}{a_\mu}\right)^{\frac{5}{2}} \frac{1}{\left[\left(\frac{Z^2}{a_\mu^2}\right)+q^2\right]^2} \tag{60}$$

$$\frac{4\pi^2\alpha}{\mu^2\omega v_e}\left|\left\langle \mathbf{k}_e \middle| e^{i\left(\frac{\omega}{c}\right)(\hat{\mathbf{n}}\cdot\mathbf{x})}\hat{\boldsymbol{\varepsilon}}\cdot\mathbf{p} \middle| 0, \mathbf{k}_\gamma \right\rangle\right|^2 = \frac{256\pi^3\hbar^2\alpha}{m^2\omega v L^3}|\hat{\boldsymbol{\varepsilon}}\cdot\mathbf{k}_e|^2\left(\frac{Z}{a_\mu}\right)^5 \frac{1}{\left[\left(\frac{Z^2}{a_\mu^2}\right)+q^2\right]^4} \tag{61}$$

$$\frac{d\sigma_{pe}}{d\Omega} = \frac{32\alpha\hbar k_e}{\mu\omega}|\hat{\boldsymbol{\varepsilon}}\cdot\mathbf{k}_e|^2\left(\frac{Z}{a_\mu}\right)^5 \frac{1}{\left[\left(\frac{Z^2}{a_\mu^2}\right)+q^2\right]^4} \tag{62}$$

$$k_e = \frac{1}{\hbar}\sqrt{2\mu(E_0 + \hbar\omega)} \tag{63}$$

$$\mathbf{q} = k_e \hat{\mathbf{\Omega}} - \left(\frac{E_\gamma}{\hbar c}\right) \hat{\mathbf{n}} \tag{64}$$

Using the spherical coordinate system shown in Figure 4.1 we can write the differential cross section explicitly in terms of polar and azimuthal scattering angles $\theta$ and $\phi$, respectively

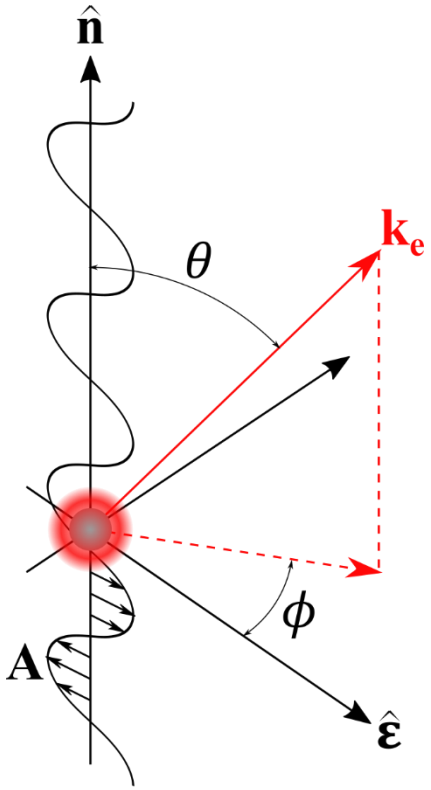


Figure 4.1 Polar and azimuthal scattering angle in differential photoelectric XS

Therefore, the differential photoelectric cross section for the k-shell ejection of a K-shell muon can be expressed as:

$$\frac{d\sigma_{pe}}{d\Omega} = \frac{32\alpha(\hbar c)^2 k_e^3}{\mu c^2 E_\gamma} |\sin\theta \cos\phi|^2 \left(\frac{Z}{a_\mu}\right)^5 \frac{1}{\left[\left(\frac{Z^2}{a_\mu^2}\right)+q^2\right]^4} \tag{65}$$

$$k_e = \frac{1}{\hbar c}\sqrt{2\mu c^2\left(E_0 + E_\gamma\right)} \tag{66}$$

$$q^2 = k_e^2 + \left(\frac{E_\gamma}{\hbar c}\right)^2 - 2k_e\frac{E_\gamma}{\hbar c}\cos\theta \tag{67}$$

The photoelectric cross sections for muonic deuterium, tritium, and alphas are calculated by numerically integrating the differential cross section by the solid angle. This was done in Matlab. The photoelectric cross section for the muonic deuterium is shown in Figure 4.2:

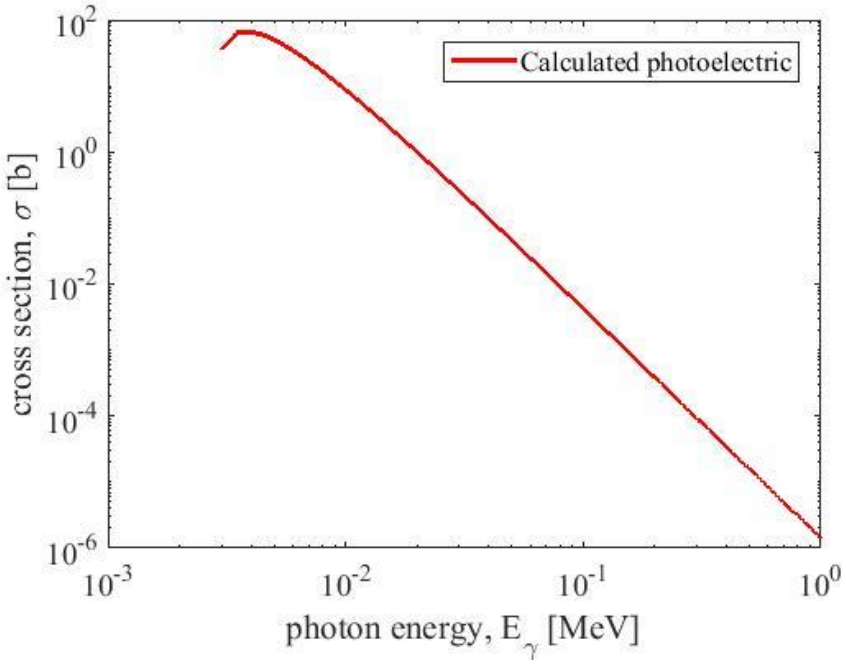


Figure 4.2 Photoelectric XS of muonic deuterium

The photoelectric cross section for muonic deuterium has an absorption edge around 4 keV and a maximum of $6.65 \times 10^{-23}\text{cm}^2$ . Muonic tritium, having the same charge, is similar as can be seen in Figure 4.3.

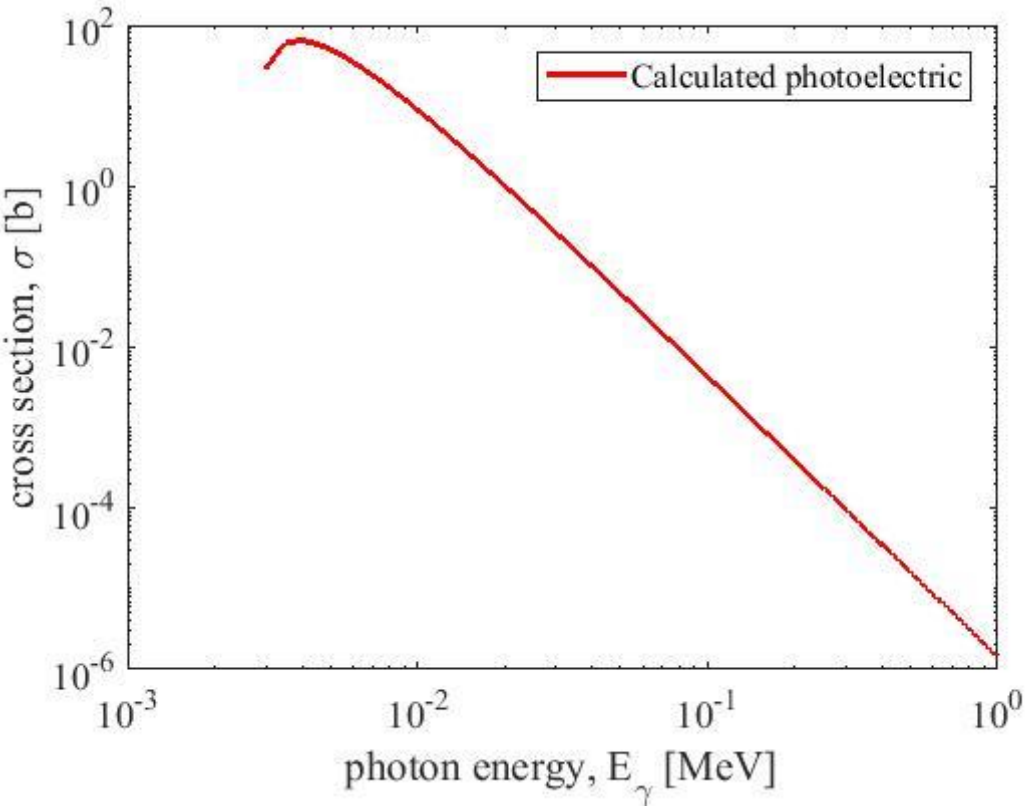


Figure 4.3 Photoelectric XS of muonic tritium

The photoelectric cross section also has an absorption edge around 4 keV and a maximum cross section of $6.46 \times 10^{-23}\text{cm}^2$ . The photoelectric cross section of the muonic alpha differs more substantially as can be seen in Figure 4.4.

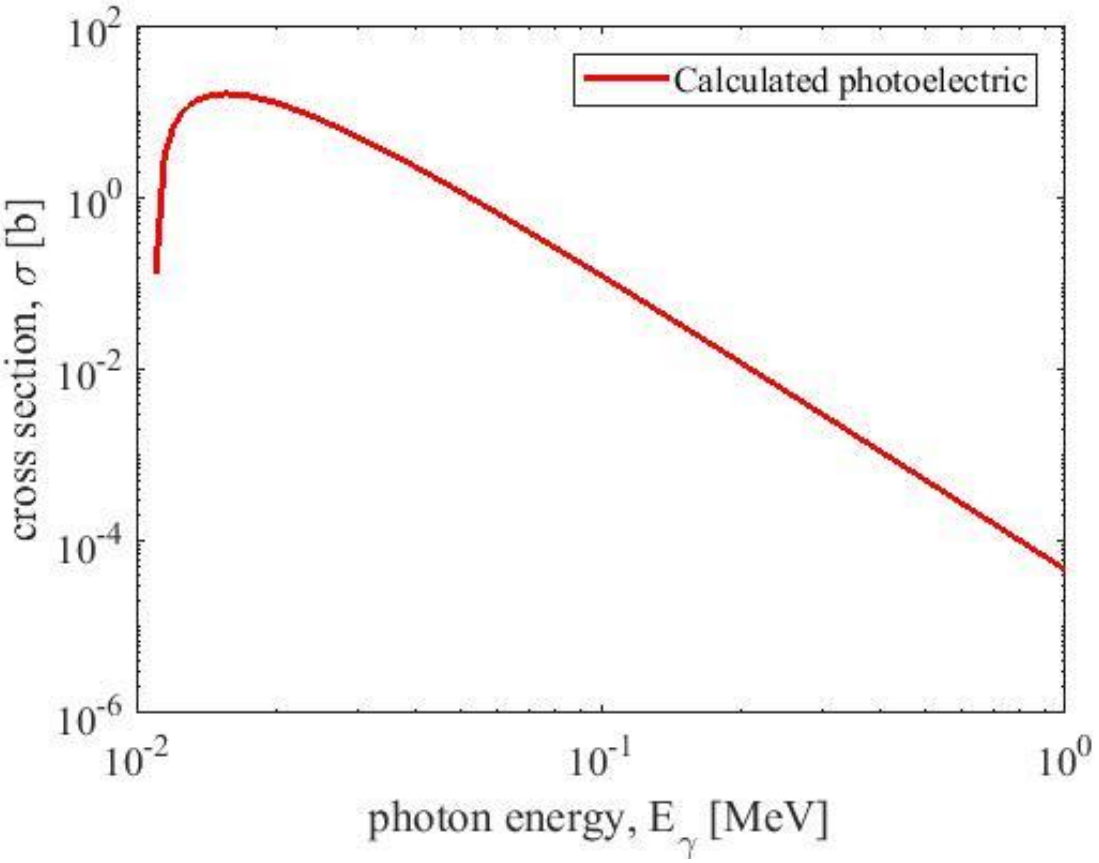


Figure 4.4 Photoelectric XS of muonic alpha

The photoelectric cross section for muonic alpha peaks around 15.5 keV with a maximum value of $1.60 \times 10^{-23}\text{cm}^2$.

## 4.2 INCOHERENT (COMPTON) SCATTERING

The Klein-Nishina formula expresses the incoherent photon scattering from a free electron (muon). The differential cross section is

$$\frac{d\sigma_{in}}{d\Omega} = \frac{1}{2}\alpha^2 r_c^2 P^2(E_\gamma,\theta)\left[P\left(E_\gamma,\theta\right) + \frac{1}{P(E_\gamma,\theta)} - \sin^2\theta\right] \tag{68}$$

Where the reduced Compton wavelength is

$$r_c = \frac{\hbar c}{mc^2} \tag{69}$$

and the kinematical factor

$$P(E_\gamma, \theta) = \frac{1}{1+\frac{E_\gamma}{mc^2}(1-\cos\theta)} \tag{70}$$

which is related to the Compton formula. Note that a reduced mass is not needed here since the charged particle is assumed to be free. After integration, the incoherent scattering cross section for free muons is obtained (Figure 4.5). Note that compared to the photoelectric effect, incoherent scattering is weak in the X-ray energy range.

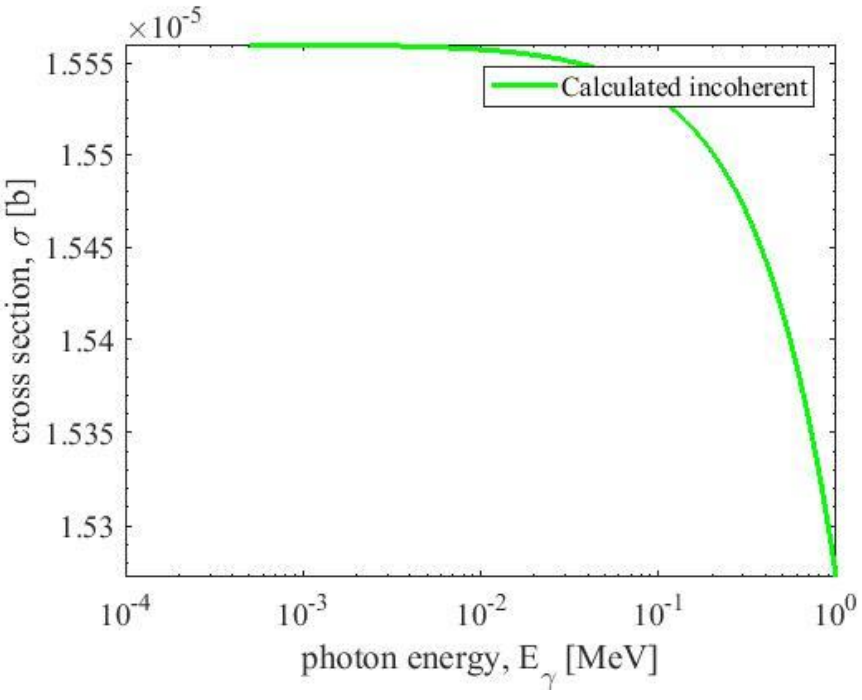


Figure 4.5 Incoherent (Compton) XS for free muons

## 4.3 TOTAL PHOTOREACTIVATION CROSS SECTIONS

The total photoreactivation cross sections, which is estimated as the sum of photoelectric and incoherent (Compton) cross sections are shown in Figure 4.6.

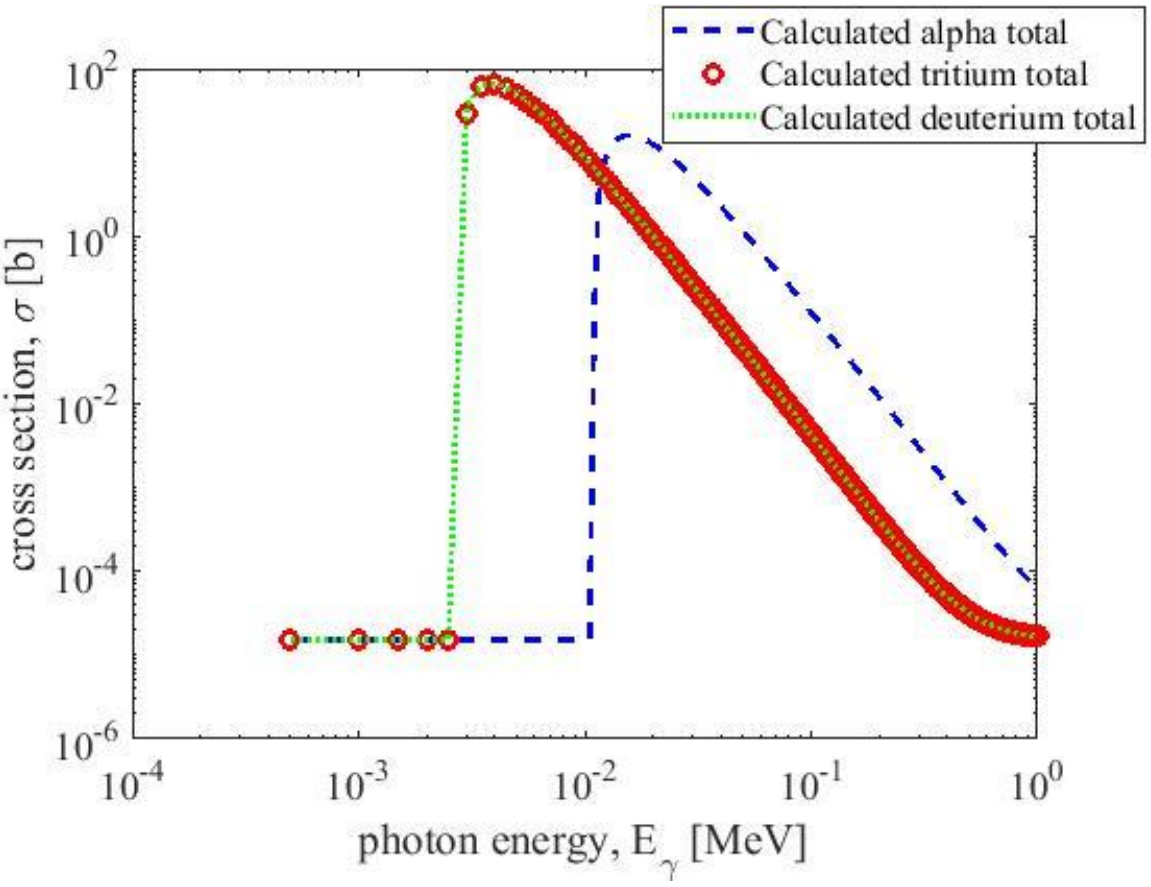


Figure 4.6 Total photoreactivation cross sections

The respective peak ionization cross sections for muonic deuterium, tritium, and alphas are attained and are represented in Table 4.1 below:

Table 4.1 Total peak muonic ionization cross sections

| | |
|---|---|
| Muonic deuterium | $6.65\times10^{-23}$ cm$^2$ |
| Muonic tritium | $6.46\times10^{-23}$ cm$^2$ |
| Muonic alpha | $1.60\times10^{-23}$ cm$^2$ |

## 4.4 REACTIVATION SOURCE STRENGTH

A continuous injection reactivation mode will be first considered. In this mode, a continuous beam of muons is injected into the reaction medium while being simultaneously irradiated by a continuous beam of X-ray photons.

The flux required to reactivate a significant fraction of alpha stuck muon is estimated as follows. If the mean time between reactivations is comparable to or less than the mean lifetime of the muon (2.2 μs) then a significant fraction of alpha stuck muons will be reactivated. This is stated as:

$$\frac{1}{\sigma\phi} = 2.2\ \mu s \tag{71}$$

$\sigma$ is the reactivation cross section and $\phi$ is the photon flux. Here, it is assumed that the photons are monoenergetic. For the peak cross sections given in Table 4.1, the fluxes that satisfy equation (71) are shown in Table 4.2.

Table 4.2 Typical reactivation photon fluxes

| | |
|---|---|
| Muonic deuterium | $6.83 \times 10^{27}\,\mathrm{cm}^{-2} \cdot \mathrm{s}^{-1}$ |
| Muonic tritium | $7.03 \times 10^{27}\,\mathrm{cm}^{-2} \cdot \mathrm{s}^{-1}$ |
| Muonic alpha | $2.85 \times 10^{28} cm^{-2} \cdot s^{-1}$ |

An order of magnitude higher flux can be expected to ionize most muonic alphas while an order of magnitude lower flux will be outpaced by muon decay. In any case, the

predicted fluxes are well above what current continuous X-ray sources are able to provide. Continuous mode reactivation will not be feasible due to restrictions in current technology and the energy requirements to produce this magnitude of fluence on a continuous operation.

**4.4.1 Probability of Ionization.** For a pulsed reactivation source, it is assumed that an infinitesimally short duration, monoenergetic X-ray pulse is shot into the medium. The probability that a single alpha stuck muon is ionized is given by:

$$P_I(15.5keV) = 1 - e^{-\Phi\sigma} \tag{72}$$

where $\Phi$ is the fluence of the pulse. An infinitesimally short pulse is approximately true provided its duration, $\Delta t$, satisfies:

$$\Delta t \ll 2.2\ \mu s \tag{73}$$

Using the values from Tables 4.1 and 4.2 it is possible to achieve an approximately 80% probability of ionization using a pulse fluence of only $10^{23}$ cm$^{-2}$. Higher fluences can achieve a higher probability of ionization at the cost of greater energy consumption. For example, a $10^{24}$ cm$^{-2}$ pulse can achieve over 99% ionization (about 20% more than $10^{23}$ cm$^{-2}$) but it uses ten times higher beam energy.

As discussed in Section 3, the concentration of alpha stuck muons reaches its maximum at $2 \times 10^{-7}$s. At this point about 90% of the muons are expected to be stuck to alphas. This is the ideal time to introduce the external reactivation source in the cycle. The fraction of muons reactivated from a single pulse is simply the peak fraction times the probability of ionization given by equation (72). For example, a $10^{23}$ cm$^{-2}$ pulse of X-rays arriving 0.2 μs after the initial muon injection pulse is expected to reactivate

approximately 72% of the muons (0.8×0.9). A $10^{24}$ $cm^{-2}$ pulse would reactivate close to 90%. If a reactivation pulse train is used, muons may be reactivated a number of times before they decay.

**4.4.2 Multiple Reactivation.** With the addition of multiple reactivation with the incorporation of a train of pulsed X-rays, it may be possible to increase the number of fusions per muon dramatically. Assuming each X-ray pulse arrives 0.2 μs after the previous pulse and assuming that the kinetics of a reactivated muon are the same as an injected source muon, except shifted by a multiple of 0.2 μs, the total number of fusions per muon can be estimated by summing powers of the reactivation fraction discussed above in a geometric series. The total fusions per muon were calculated from reactivation X-ray fluences between $10^{22}$ and $10^{24}$ $cm^{-2}$ per pulse. The results are shown in Figure 4.9:

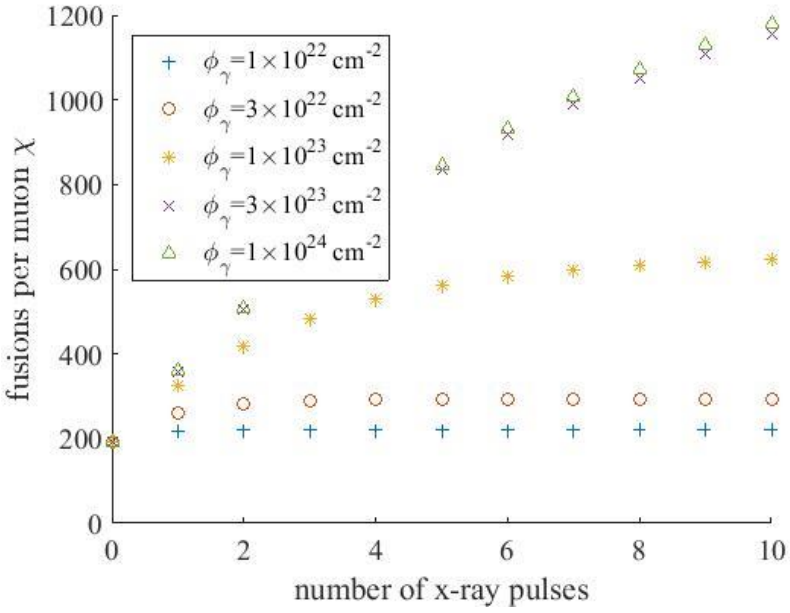


Figure 4.7 Fusions per muon as a function of number of pulses

It can be observed that at a reactivation fluence of $10^{22}$ $cm^{-2}$, the number of fusion events only increases marginally from just below 200 to just above 200. At a reactivation fluence of $3\times10^{22}$ $cm^{-2}$ the number of fusion events per muon reaches around 300 after one pulse. At a reactivation fluence of $10^{23}$ $cm^{-2}$ the number of fusion events exceeds 600 after 3 pulses. At a reactivation fluence of $10^{24}$ $cm^{-2}$, the number of fusion events reaches 1200 fusion events per muon after ten pulses. This clearly demonstrates that an external reactivation source can effectively mitigate alpha sticking and increase the muon economy for fusion.

In order to select an adequate source, the X-ray attenuation and energy loss needs to be taken into consideration. The approximations used up to this point assume that the photon beam experiences no attenuation or scattering in the medium. If proven that the photon flux and energy does not change by a substantial margin from energy loss, these assumptions are reasonable. Radiation transport calculation that show this are presented in appendix A.

## 4.5. MUON SOURCE AND PHOTON BEAM TARGET

The first setup of the catalytic process is the introduction of the muons into the target medium. An adequate fuel medium needs to be selected for the most optimal environment to facilitate the most opportunities for fusion reactions to take place. A target medium of either superfluid hydrogen or deuterium can be ruled out due to a phenomenon called Coulomb explosions [18]. This violent process occurs when energetic pulsed sources are introduced into the superfluid or super cooled medium, causing rapid charge separation and destabilization of the medium [19]. Ideal media for the use of

muons in the fusion process would be a cooled deuterium tritium mixture. A DT mixture of 50% tritium and 50% deuterium was chosen for the fuel mixture.

Typical accelerator-based muon sources have extremely high energy demands and space requirements. This creates a unique requirement for a practical muon source in order to make muon catalyzed fusion economical.

With the advances made in Wakefield acceleration, hypothetical bright muon sources have been proposed [20,21]. Wakefield accelerators are relatively compact particle accelerators that can reach energies in the GeV range. A selection of possible muon source parameters is given in Table 4.4.

Table 4.3 Selected parameters for muon source

| | |
|---|---|
| Muons per pulse | $10^{15}$ |
| Selected Energies (MeV) | 1, 10 |
| Pulse duration (ps) | 200 |
| Beam radius (mm) | 1 |
| Repetition Rate | 500 Hz |
| Fusions per muon | 1200 |
| Thermal power (MW) | 1600 |

Assuming a perfectly well collimated muon beam, the spatial distribution of fusion events in the medium is largely determined by muon stopping and straggling. The spatial extent of the resultant stopped muons defines a target volume of the medium that the X-ray beam must hit. A Monte Carlo simulation was undertaken in order to identify the distance travelled by the source muons into the media, their spatial distribution due to

straggling, as well as where the highest concentration may reside. The Monte Carlo software called, MCNP (Monte Carlo N Particle Transport) is used to simulate the straggling process. The simulations are covered in detail in appendix B. The resulting target sizes for 10 MeV and 1 MeV muons are on the order of a few cm and a few mm, respectively.

At both of these incident energies, it can be concluded that although a large concentration of the source muons stops in one region, a large amount of muons are randomly dispersed in the medium. All muons in the medium will contribute to fusion reactions but only muons in the target region can be reactivated. Increasing the X-ray beam size while keeping the fluence high ($10^{23}$-$10^{24}$ $cm^{-2}$) comes at the cost of proportionally higher reactivation source energy costs. Thus, geometric effects and target size play an important role in the selection of the injected muon energy and the design and optimization of the system as a whole. They also play a large role in selecting a hypothetical external reactivation source, as various accelerator based brilliant light sources are confined to their target size of interaction.

## 4.6 EXTERNAL REACTIVATION SOURCE SELECTION

The external reactivation source selection can now be selected as a pulsed source. The inadequacy and realistic nature of a continuous source, as previously discussed is a reason for this along with the previously discussed limitations for such a strategy for external reactivation. From the previous discussion a pulsed X-ray source should have the following characteristics.

i. Fluence of $10^{22} – 10^{24}$ photons per pulse per $cm^2$, in order to achieve an improved muon economy

ii. Beam size on order of mm to cm

iii. Energy of incident photon should be about 15.5 keV

Current bright X-ray sources may not be able to meet these requirements. Typical bright photon sources include synchrotrons and free electron lasers. These sources have extremely high energy demands. Wakefield source technology, though less mature, is capable of producing high flux output at relatively low energy costs. Three possible sources for external reactivation are as represented in Table 4.4

Table 4.4 Bright X-ray source parameters

| | EU XFEL | ESRF | Wakefield X-ray source |
|---|---|---|---|
| Incident Beam Intensity | $10^{15}$ per pulse | $10^{18}$ $cm^{-2}$ $s^{-1}$ $mrad^{-2}$ | $10^{26}$ $cm^{-2}$ |
| Pulse Durations | 100 fs | 0.1 as | 40 fs |
| Beam size between | 100-1000 nm | 57×10 μm | 1 mm |
| Photon Energy range | 0.5 keV-900 GeV | 5 keV-90 keV | 5 keV -40 GeV |
| Repetition Rate | 10 Hz | 3 kHz [26] | 0.5 kHz [25] |

The values of Table 4.5 represent a synchrotron (European Synchrotron Radiation Facility or ESRF), a free electron laser (the European X-ray Free Electron Laser or EU XFEL in Hamburg) and a Wakefield design [25]. While the synchrotron and free electron laser are capable of delivering extremely high fluences when normalized by their beam

area, the beam area itself is probably too small to be of use in a situation where muons are stopping in a region greater than a few square mm in area. This presents itself with possible energy density issues, however the energy economy of this process will next be brought to focus.

# 5. ENERGY ECONOMY

With the principle of muon reactivation by an external X-ray source demonstrated, the question becomes, how much energy generated from fusion reactions will need to be invested back into the reactivation source? An energy balance equation is given below:

$$Q_{out} = N_\mu \chi(\Phi_\gamma, N_P) Q_f \epsilon_{th} - N_\mu C_\mu - N_p C_{\gamma,P}(\Phi_\gamma) \quad (74)$$

$Q_{out}$ is the net energy production. The first term on the right-hand side of the equation is the electrical energy generated by fusion. $N_\mu$ is the number of muons injected in a single pulse. $\chi$ is the number of fusions per muon, which is a function of the photon pulse fluence, $\Phi_\gamma$, and the number of pulses, $N_P$. $Q_f$ is the average binding energy released per fusion reaction and $\epsilon_{th}$ is the thermal efficiency in converting thermal energy in the coolant into electrical energy. The second term on the right hand side of the equation is the cost of generating source muons. $C_\mu$ is the per muon energy cost. The last term is the cost of generating reactivation pulses. $C_{\gamma,P}$ is the energy cost to produce a single X-ray pulse including losses. It is a function of the fluence per pulse.

Diving both sides of the equation by $N_\mu$ gives:

$$Q_{out}/N_\mu = \chi(\Phi_\gamma, N_P) Q_f \epsilon_{th} - C_\mu - N_p C_{\gamma,P}(\Phi_\gamma)/N_\mu \quad (75)$$

Breakeven is achieved when there is no net energy gain ($Q_{out} = 0$). This can be expressed as the maximum allowable cost of the external reactivation pulse.

$$C_{\gamma,p} \leq \frac{N_\mu}{N_p}\left(\chi Q_f \varepsilon_{th} - C_\mu\right) \tag{76}$$

Provided the energy cost of the external source obeys Equation (76), the system can generate net power or at least break even. Even if electrical power could be converted into X-rays with zero losses, the cost of the X-ray pulse will be at least as great as the energy contained in all of the X-rays. In other words,

$$E_\gamma \Phi_\gamma A \leq C_{\gamma,p} \tag{77}$$

$E_\gamma$ is the X-ray energy and $A$ is the beam area. Putting equations (76) and (77) together

$$E_\gamma \Phi_\gamma A \leq \frac{N_\mu}{N_p}\left(\chi Q_f \varepsilon_{th} - C_\mu\right) \tag{78}$$

which means that the number of muon injections is given by

$$N_\mu \geq \frac{N_p E_\gamma \Phi_\gamma A}{\chi Q_f \varepsilon_{th} - C_\mu} \tag{79}$$

The thermal energy generated by a single muon injection would therefore be:

$$\chi Q_f N_\mu \geq \frac{\chi Q_f N_p E_\gamma \Phi_\gamma A}{\chi Q_f \varepsilon_{th} - C_\mu} \tag{80}$$

After establishing the following conditions using the values in Table 5.1, the number of muons injected per pulse would need to be greater than about $10^{20}$ and power generated would be greater than 300 GJ. In essence, the cost of an external reactivation is so great that the fusion density would need to be unrealistically high to help supply power to it.

Table 5.1 Breakeven criterion parameters

| | |
|---|---|
| $\chi$ | 1200 fusions per muon |
| $Q_f$ | 17 MeV per fusion |
| $\varepsilon_{th}$ | 33% thermal efficiency |
| $C_\mu$ | 5000 MeV per muon |
| $A$ | 1 $cm^2$ |
| $N_p$ | 10 reactivation pulses |

Considering the small target size, the massive energy release, and the timescale of the pulse, the resulting power density grossly exceeds that of a conventional power reactor [27]. In fact, at such high energy densities, many of the assumptions in the models would be wrong. Perhaps most significantly, the medium would rapidly heat into a plasma rendering the muons useless. Therefore, while non-breakeven external reactivation is a possible in theory, breakeven power from muon catalyzed fusion is a practical impossibility.

# 6. CONCLUSION

A detailed modeling study of muon catalyzed fusion was performed to investigate the possibility of incorporating an external X-ray source to reactivate muons bound to alpha particles. These so-called alpha stuck muons are considered to be the primary obstacle to breakeven muon catalyzed fusion power. Using point kinetics, analytical interaction cross sections and Monte Carlo simulation, the basic parameters for a hypothetical X-ray reactivation source were determined.

It appears that reactivation of alpha stuck muons is possible in principle. A sufficiently intense 15 keV X-ray source would be able to effectively ionize alpha stuck muons and reintroduce them back into the catalysis cycle, increasing the number of fusions per muon by a factor of several times the previous limit.

Pulsed injection and reactivation appears to be a more efficient approach to reactivation than continuous reactivation as roughly 90% of muons are predicted to become bound on byproduct alphas 0.2 μs after muon injection. Per photon, a greater number of muons can be reactivated from an intense pulse than from a continuous beam of photons.

An analysis of the energy economy of such a system shows that energy breakeven can only occur when operated on a GJ per pulse scale. The required muon source strength would need to be several orders of magnitude more intense than current muon sources and even hypothetical designs can provide. Meanwhile, the energy densities predicted in a breakeven scenario are at such a high scale that many of the physical assumptions made in the models become unrealistic.

# APPENDIX A.

# MCNP SIMULATION: X-RAY ATTENUATION AND ENERGY LOSS

MCNP or Monte Carlo N Particle is the radiation transport code that will be utilized for this analysis. In order to pursue an X-ray attenuation and energy loss analysis on MCNP, the F2 Surf flux tally function needs to be invoked. This tally will identify the change in the flux of photons from the x-ray reactivation source when it passes completely through the medium. The two surfaces that will be selected are the source surface and the opposite surface at the adjacent end of the DT medium's volume. The incident photon energy will be the photo-muon reactivation energy from the muonic alpha, 15.5keV. The energy range that will be analyzed is 0keV to 15.5keV and 1 billion photons will be transported in the tally. The setup can be visualized in Figure A.1:

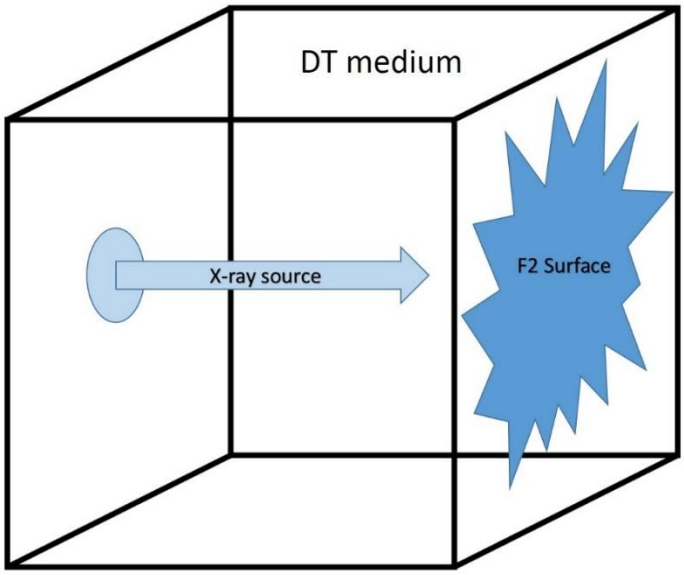


Figure A.1: X-ray Attenuation run visualized

After processing the MCNP simulation run, the surface flux analysis of the exit surface shows the following distribution in the change of the flux in Figure A.2:

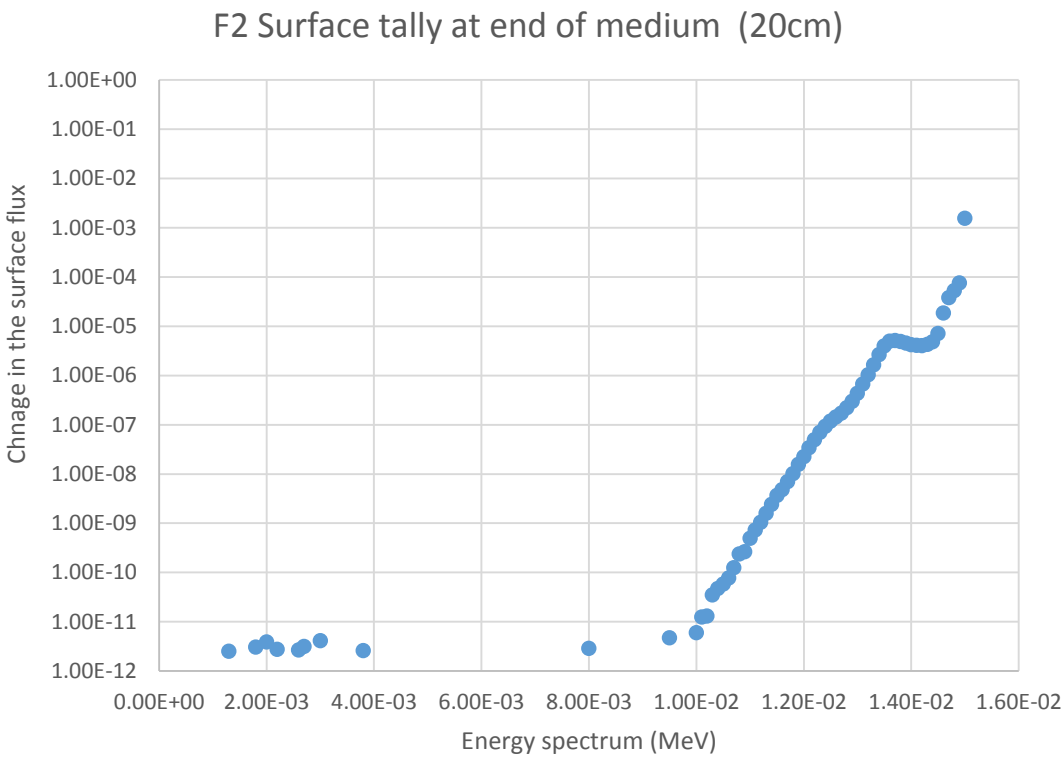


Figure A.2 F2 tally results

This plot of the surface flux across the energy range shows that there is little to no change in the flux as it passes through the entire medium. The ratio of down scattered photons to incident photons is 1,191,311 to 1,000,000,000 or 0.0012. The ratio of the uncollided flux to the incident flux is 998,808,765 to 1,000,000,000 or 99.881. The energy loss by Compton scatter is 0.253keV, therefore this removes the need for the consideration of inherent (Compton) scattering cross section as a major source for energy loss from muons and electrons. This is also supplemented by the fact that the photoelectric cross sections dominate the total photoreactivation cross section overall. At

the very least, the incident photon energy can be increased slightly to account for the 0.253keV loss. This dictates that for a hypothetical external reactivation source to reactivate alpha stuck muons in a reactor sized setting, for every meter of width for such a system, the incident energy will have to by increased by an order of 0.253keV.

# APPENDIX B.

# MCNP SIMULATION: MUON SOURCE INTRODUCTION

In order to demonstrate that the selected muon source can ‘slow down’ into the epi-thermal energy range required for ‘sticking’ or the radiative capture (4eV-25eV) on the DT medium, a MCNP simulation is setup to demonstrate this [20]. This will show the thermalization process that muons under go when they are exposed to hydrogen isotopes and alpha particles at an epi-thermal energy. This will be done through the use of PTRAC card in order to estimate the range of muons into the DT medium. A PTRAC run allows the tracking of each individual particle in a MCNP run. This allows data such as the position of each particle to be recorded once it reaches the desired cutoff energy established in the run. In order to run multiple cores, the Linux platform Cygwin had to be used and an MPI had to be implemented since although MCNP6.2 is capable of muon transport, it is not capable of running multiple cores for muon transport. As a setup for the analysis of the muon epi-thermalization, a cube of liquid DT fuel mixture is selected with an inward pointing monoenergetic beam source of muons being injected into the system visualized in Figure B.1:

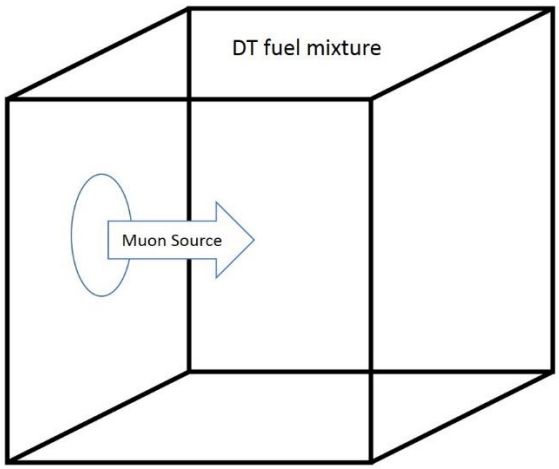


Figure B.1 MCNP PTRAC run visualized

This geometry was established as an arbitrary scenario for muon injection into a DT mixture for a fusion system. This scenario removes the need for analysis on the muon interactions with regions of varying density as within this cube the DT medium density is assumed to be isotropic across the entire region of interaction (everything within the cube). The two cells created in the input card consist of everything outside the cube and everything inside the cube, with everything outside the cube given an importance value of zero and everything inside the cube given an importance value of one.

After the cell definition, the surfaces are defined and the media is given a size of 20x20x20cm. A fusion system would typically be much larger than this, however a scale of this size will suffice in order to demonstrate the mechanics of the muon in the DT media. As stated before, a monoenergetic, muon beam source was created pointing into the cube. It was chosen to be monoenergetic for two reasons. Firstly, in order the represent a realistic muon source it was decided to simulate an accelerator-based muon source [22,30]. These are typically in the GeV to TeV scales of energies however can be tunable to much lower energy magnitudes, and are typically monoenergetic in nature. Secondly, in typical muon experiments the source of muons are cosmic muons.

These typically have energies ranging from keV to GeV [20]. In order to pick a realistic energy to allow for the thermalizing of the muons to occur which typically takes between ($10^{-10}$ s - $10^{-14}$ s [20]), 10MeV was selected to allow for this to occur while maintaining a high enough energy to penetrate the medium sufficiently. MCNP6.2 uses electron stopping power calculate this slowing down into the thermalizing energies. The muon transport mode is enabled and the material card includes the deuterium and tritium concentrations in the media for the respective interactions. The concentrations are

arbitrarily selected to be 50% deuterium and 50% tritium for an even population of the fuel particles. A lower bound energy card cut off is implemented at 25eV due to this being the start of the epi-thermal zone a muon reaches before being radiatively captured. The PTRAC feature is enabled and one hundred thousand particles were run. Due to the particle limitation on the PTRAC feature, a particle number of 100000 is selected for transport. This is due to the file size of the generated tracked particles; however, this will be adequate for representing a trend in the order of magnitude of the necessary target size for the photon beam to interact with.

After the run, the muons seemed to exhibit the expected behavior of a typical beam source into a media. As it can be seen below a representation of the X-Y plane in Figure B.2 and X-Z plane in Figure B.3 of the media:

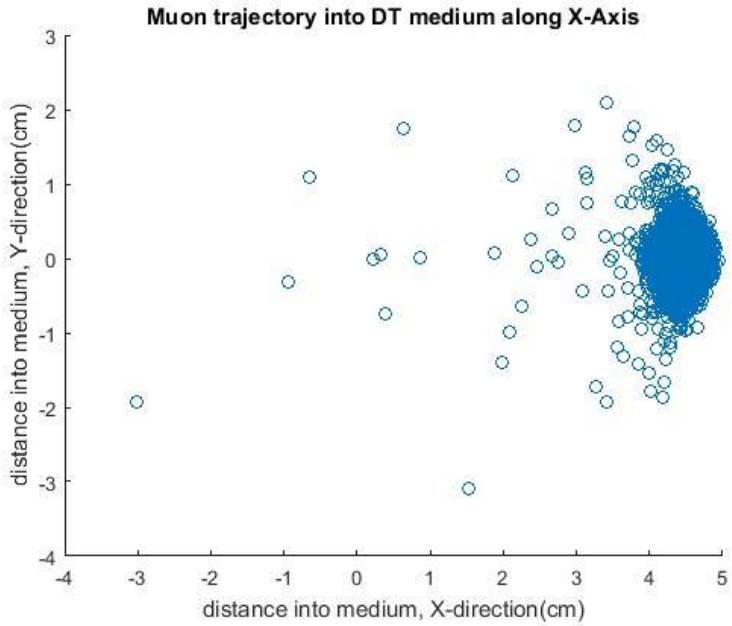


Figure B.2 10MeV PTRAC run in X-Y plane

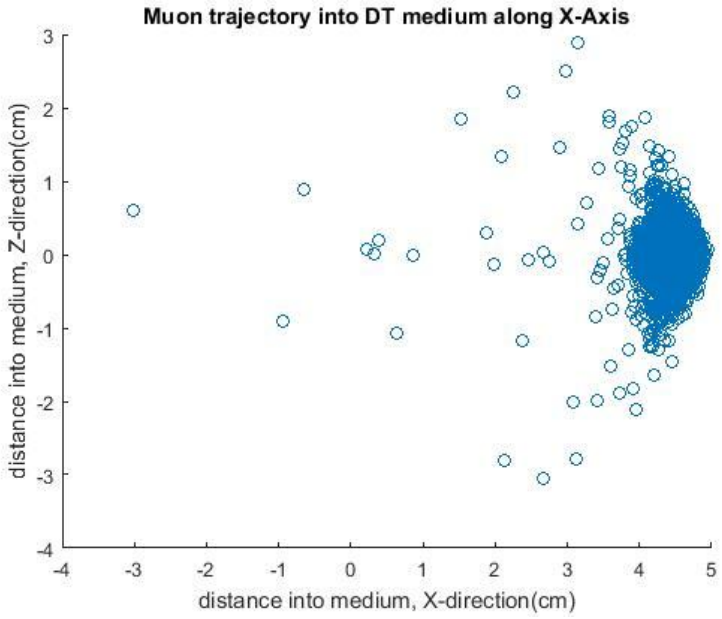


Figure B.3 10MeV PTRAC run in X-Z plane

A common trend can be observed between the two orientations. That is that most of the 10 MeV muons from the Wakefield source ‘slow down’ to the epi-thermal energy range between the distances of 4 to 5cm into the DT medium. At the incident energy no backscattering can be observed as well however the majority of the particle population can be observed stopping in a rough 1cm by 2cm area specifically in the X-Y and X-Z orientation. There appears to be straggling in the Y-direction source size deviation being +1cm, this is taken for particles at the edge of the majority cluster. This deviation is calculated to be 0.244978 radians or 14.04° straggling of the X-axis. The Y-Z plane in Figure B4 below shows similar trends:

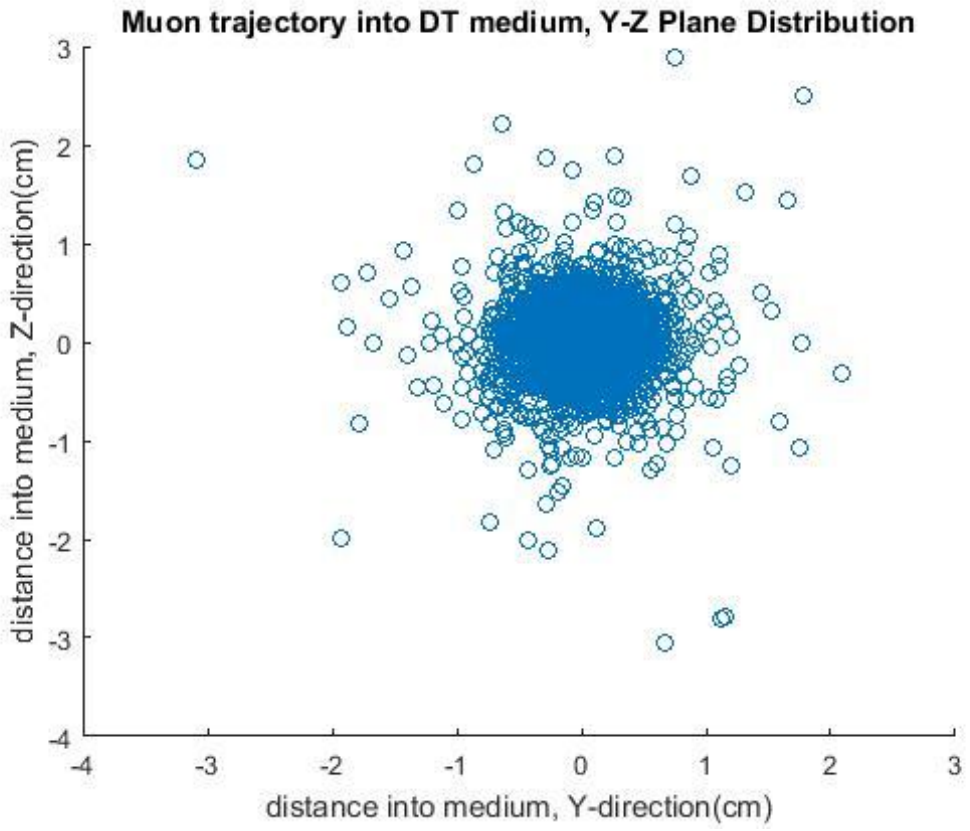


Figure B.4 10MeV PTRAC run in Y-Z plane

The majority of the muon population in this plane is roughly confined within a 2cm by 2cm region, thus in a volumetric sense most of the source particles that are introduced are within a 2 by 2 by 1cm ($4cm^3$) volume in the DT mixture once the epi-thermal energy range is reached. This clears shows that at a 10 MeV incident energy, the target size for reactivation is on the order of cm. Running the PTRAC simulation at a lower muon energy of 1 MeV yields a slightly more collimated result. The pulse seems to reach the epi-thermal range without much straggling. This is characteristic for a lower energy wakefield source. This can be seen below a representation of the X-Y plane in Figure B.5:

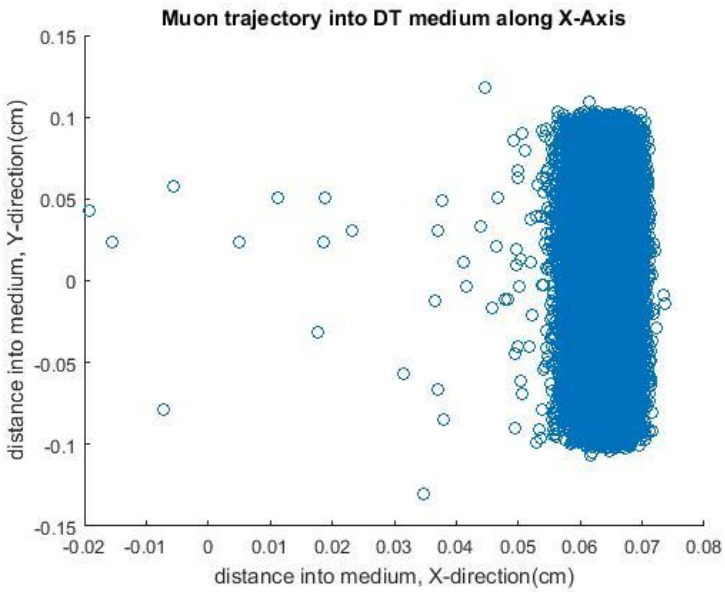


Figure B.5 1MeV PTRAC run in X-Y plane

The majority of the muon flux, after slowing down into the epi-thermal energy range, is between the 0.055cm and 0.072cm in the X-direction and between 0.11cm and -0.11cm in the Y-direction. The trends are similar in the X-Z plane in Figure B.6:

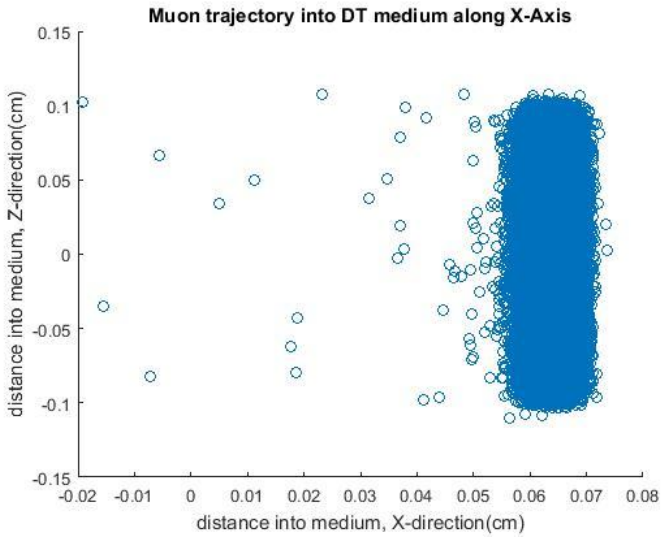


Figure B.6 1MeV PTRAC run in X-Z plane

Similarly, the muon flux is between the 0.055cm and 0.072cm in the X-direction and between 0.11cm and -0.11cm in the Y-direction this shows that the pulse does not straggle over a wider area in the DT medium at this energy. There appears to be a slight outward scattering due to the Y-direction source size deviation being +.01cm, this is taken for particles at the edge of the majority cluster. This deviation is calculated to be a 0.179853 radian drift or a 10.3° drift of the X-axis. This can be seen in the Y-Z plane in Figure B.7:

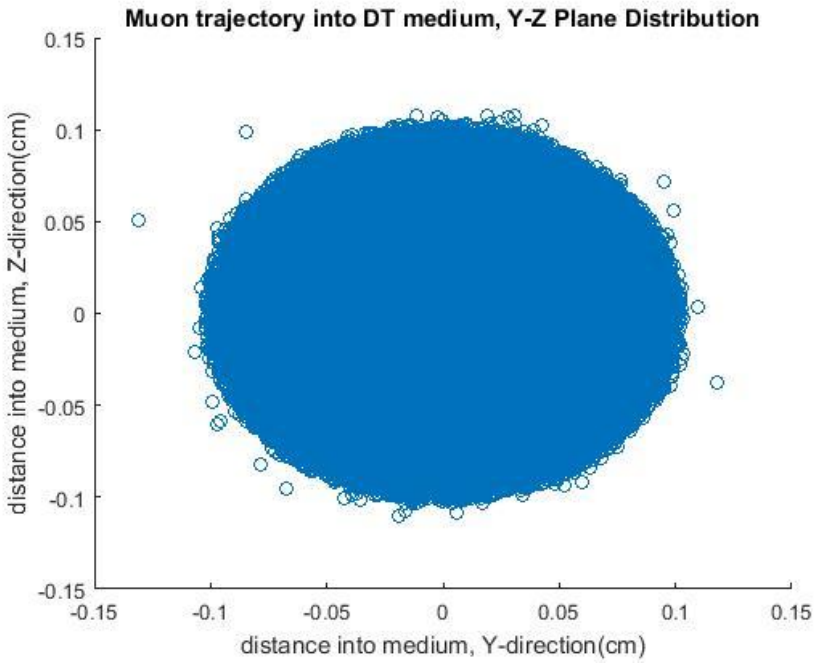


Figure B.7 1MeV PTRAC run in Y-Z plane

The muon population at 1MeV for the Y-Z plane is roughly confined within a 0.1cm by 0.1cm region. Thus, in a volumetric sense most of the source particles that are introduced are within a 0.2 by 0.2 by 0.017cm ($0.00068cm^3$ or $0.68mm^3$) volume in the DT mixture once the epi-thermal energy range is reached. The target size for the reaction

substantially decreases from the cm scale to the mm scale when the incident muon energy on injection is 1MeV. At both these incident energies of 1MeV and 10MeV, it can be concluded that although a large concentration of the source muons conglomerates in one area, a large amount of muons still disperses in into the medium. All of which are still useful for fusion reactions and are in fact transported into the media as they reach the 'sticking' or radiative capture energy ranges of 4eV to 25eV. This however opens the possibility to account for all the source muons in the medium, if the volume of focus is expanded from the $mm^3$ scale to the $cm^3$.

The sticking or radiative capture of muons in the system is dependent on their thermalization. The muon source, driven by Wakefield acceleration, will produce muon pairs up to 10GeV at a flux of $5x10^{17}$ pairs/pulse/$cm^2$/sr, however this setup only requires energies in the MeV region [8]. The average muonic stopping power at 1MeV of liquid hydrogen is 4.103MeV $cm^2/g$ [22]. The DT mixture selected is comparable to this. In order to calculate the necessary media size and confinement vessel size for this system the radial direction needs to be calculated using the following relationship between the energy loss and stopping power [23]:

$$\Delta x(cm) = \frac{S_\mu \rho}{E_l} = \frac{4.103 MeV \cdot cm^2 \cdot 0.225 g}{1 MeV \cdot g \cdot cm^3} = 0.92 cm \qquad (81)$$

Using this relation, the 'stopping' distance into the medium is calculated above. With this sort of calculated distance, it is possible to upscale a theoretical vessel size based on incident muon energy. This scale of size still brings up the possible concern of a high energy density due to the scale of such a flux on such an area.

# REFERENCES


[1] INTERNATIONAL ATOMIC ENERGY AGENCY, Utilization of a Network of Small Magnetic Confinement Fusion Devices for Mainstream Fusion Research, IAEA-TECDOC-1807, IAEA, Vienna (2016).

[2] R. Pitts, "Fusion: the way ahead", Physicsworld, 2006. [Online]. Available: https://physicsworld.com/a/fusion-the-way-ahead/.

[3] V. Bezchastnov, P. Schmelcher and L. Cederbaum, "Bound states of negatively charged ions induced by a magnetic field", Physical Review A, vol. 61, no. 5, 2000. Available: 10.1103/physreva.61.052512

[4] S. Alexander, P. Froelich and H. Monkhorst, "Nuclear fusion rates of muonic molecular ions", Physical Review A, vol. 41, no. 5, pp. 2854-2857, 1990. Available: 10.1103/physreva.41.2854.

[5] Muon catalyzed fusion, Katsuhiko Ishida, Kanetada Nagamine, Teiichiro Matsuzaki and Naritoshi Kawamura, Published 9 July 2003 • Journal of Physics G: Nuclear and Particle Physics, Volume 29, Number 8

[6] D. Ceperley and B. Alder, "Muon–alpha-particle sticking probability in muon-catalyzed fusion", Physical Review A, vol. 31, no. 4, pp. 1999-2004, 1985.

[7] Eliezer, S. and Henis, Z. (1994). Muon catalyzed fusion-An Energy production perspective. Fusion Technology, 26.

[8] A. Frolov, "Muon sticking probabilities for the symmetric muonic molecular ions ddμ and ttμ", Physics Letters A, vol. 291, no. 4-5, pp. 274-280, 2001. Available: https://doi.org/10.1016/S0375-9601(01)00729-0.

[9] E.J. Weinberg, et.al., Physical Review D54, Particles and Fields, 1996

[10] E. Sheely, "THEORETICAL STUDY OF THE EFFECTS OF DI -MUONIC MOLECULES ON MUON-CATALYZED FUSION", PhD, Air Force Institute of Technology, 2012.

[11] A. Frolov, "Muon sticking probabilities for the symmetric muonic molecular ions ddμ and ttμ", Physics Letters A, vol. 291, no. 4-5, pp. 274-280, 2001. Available: 10.1016/s0375-9601(01)00729-0.

[12] C. Stodden, H. Monkhorst, K. Szalewicz and T. Winter, "Muon reactivation in muon-catalyzedd-tfusion from accuratep-He+stripping and excitation cross sections", Physical Review A, vol. 41, no. 3, pp. 1281-1292, 1990. Available: 10.1103/physreva.41.1281.

[13] R. Gheisari and A. Avazpour, "Nuclear fusion rate for ddμ muonic molecule", International Journal of Quantum Chemistry, vol. 108, no. 2, pp. 378-382, 2007. Available: 10.1002/qua.21530.

[14] M. Fujiwara et al., "Resonant Formation of dμt Molecules in Deuterium: An Atomic Beam Measurement of Muon Catalyzed dt Fusion", Physical Review Letters, vol. 85, no. 8, pp. 1642-1645, 2000. Available: 10.1103/physrevlett.85.1642.

[15] K. Nagamine, Contribution of Muon Catalyzed Fusion to Fusion Energy Development, 1st ed. Sendai: Muon Science Laboratory RIKEN, Meson Science Laboratory High Energy Accelerator Research Organization (KEK), Department of Physics, Graduate School of Science Tohoku University, 2014, pp. 1-5.

[16] Modern Quantum Mechanics by J. J. Sakurai

[17] K. Deb and H. Jain, "An Evolutionary Many-Objective Optimization Algorithm Using Reference-Point-Based Nondominated Sorting Approach, Part I: Solving Problems With Box Constraints", IEEE Transactions on Evolutionary Computation, vol. 18, no. 4, pp. 577-601, 2014. Available: 10.1109/tevc.2013.2281535.

[18] D. Anagnostopoulos, P. Indelicato and D. Gotta, "First Direct Observation of Coulomb Explosion during the Formation of Exotic Atoms", *Physical Review Letters*, pp. 1-5, 2000. Available: DOI: 10.1103/PhysRevLett.84.4573.

[19] J. Jortner and I. Last, "Nuclear Fusion Driven by Coulomb Explosion of Molecular Clusters", ChemPhysChem, vol. 3, no. 10, pp. 845-848, 2002. Available: 10.1002/1439-7641(20021018)3:10<845::aid-cphc845>3.0.co;2-p.

[20] V. Kulhar, "Muonium/muonic hydrogen formation in atomic hydrogen", Pramana, vol. 63, no. 3, pp. 543-551, 2004. Available: 10.1007/bf02704482.

[21] B. Rao, J. Jeon, H. Kim and C. Nam, "Bright muon source driven by GeV electron beams from a compact laser wakefield accelerator", *Plasma Physics and Controlled Fusion*, vol. 60, no. 9, p. 095002, 2018. Available: 10.1088/1361-6587/aacdea.

[22] D. GROOM, N. MOKHOV and S. STRIGANOV, "MUON STOPPING POWER AND RANGE TABLES 10 MeV–100 TeV", Atomic Data and Nuclear Data Tables, vol. 78, no. 2, pp. 183-356, 2001. Available: 10.1006/adnd.2001.0861.

[23] D. Casas, M. Barriga-Carrasco, A. Andreev, M. Schnürer and R. Morales, "PROTON STOPPING POWER OF DIFFERENT DENSITY PROFILE PLASMAS", Acta Polytechnica, vol. 55, no. 2, pp. 76-80, 2015. Available: 10.14311/ap.2015.55.0076.

[25] Najmudin Z *et al*. 2014, Compact laser accelerators for X-ray, phase-contrast imaging. *Phil. Trans. R. Soc. A*

[26] "Technical specifications- ESRF beamline 8", *ESRF - The European Synchrotron*, 1994. [Online]. Available: https://www.esrf.eu/UsersAndScience/Experiments/CRG/BM08/Users/tech_spec.html.

[27] Aris.iaea.org. (2019). *ARIS - Technical Data*. [online] Available at: https://aris.iaea.org/sites/core.html?fbclid=IwAR0uQAYbmE8N66CGhK7qYIl4nIO9RsF9jMn4SdRBAjzHH55Um5aEfXjkhcQ.

# VITA

Nishant Raghav Pillai was born in Newark, Delaware. In May 2020 he received has MS degree in Nuclear Engineering from Missouri University of Science and Technology. He received his Bachelor of Science in Nuclear Engineering from Missouri University of Science and Technology in May 2017.